공학박사학위논문

Organic Imaging Probe Activated by Hypoxia and Ultrasound

저산소 조건과 초음파에 의해 활성화되는 유기물질 기반 조영물질

2019 년 8 월

서울대학교 대학원

재료공학부

정 인 재

Abstract

Organic Imaging Probe Activated by Hypoxia and Ultrasound

In Jae Chung

Department of Materials Science and Engineering

College of Engineering

Seoul National University

Effective method of imaging disease for accurate diagnosis and early treatment of disease has been demanded. Functional imaging could observe molecular events occurring in the disease at the cellular level, so effective imaging is possible even in the early stages of disease, which is difficult to judge disease with anatomical imaging methods. An ample amount of research has been executed for molecular imaging to diagnose tumor by using specific environment that appears around tumor cell. Stimulus-sensitive material allows selective imaging of disease or drug delivery by the tumor

microenvironment. The stimulus-sensitive substance refers to a substance whose physical properties are changed or chemically altered by the microenvironment expressed in a disease in the body. The use of a stimulus-sensitive material allows selective imaging of disease and delivery of therapeutic agents by the environment expressed around cancer.

In this study, we developed a fluorescence activated probe using a stimulus-sensitive material. In case of fluorescence imaging, background noise should be suppressed as much as possible. When the fluorescent material is used without any action, it is difficult to obtain accurate images because of low signal-to-noise. Fluorescence quenching takes place when the fluorescence dye and quencher are in proximity. Activatable image starts by bond cleavage between the fluorescent material and the quencher by cell microenvironments such as enzyme and pH.

The self-immolative materials are collapsed by single triggeric event to release multiple end group. In chapter 2, we have developed a dendrimer shaped activatable optical imaging agent that selectively activates fluorescence under hypoxic conditions using a self-immolative structure. Self-quenched optical imaging probe was synthesized by conjugation of fluorescence dye to the end of the dendron. As the nitro group was reduced to an amine group under hypoxic condition, the fluorescence was recovered

due to cascade degradation and release of fluorescence dye. The imaging of hypoxic conditions is possible through the increase of fluorescence intensity. Unlike conventional hypoxia sensitive imaging, multiple fluorescence was released by the single trigger. It provide signal amplification characteristic, thus showing possibility of effective diagnostic for hypoxic tumor.

External stimuli can induce selective microenvironmental changes at the target site. In chapter 3, it was confirmed that the drug delivery efficiency is enhanced by increasing the cell permeability at the target site by ultrasonic waves and microbubbles. Microbubbles can induce temporary permeabilization of cell membranes by forming strong flow (microjet) by ultrasonic irradiation. When microbubbles-drug carrier complex were injected into the body, ultrasound induced selective drug delivery is possible because cell permeability is selectively increased at the site irradiated with ultrasound. By the in vitro experiment, it was confirmed that ultrasound-mediated increase of cell permeability in the presence of microbubble complex. Through in vivo experiments, ultrasound-induced enhancement of drug delivery efficiency was confirmed by fluorescence imaging.

Keywords : Stimuli-Sensitive material, hypoxia, self-immolative structure, optical imaging, microbubble, ultrasound, self-aggregate

Student Number **:** 2011-23323

Contents

List of Tables and Schemes

List of Figures

Chapter 1.

Introduction

1.1. Imaging modalities

Several imaging methods have been used to effectively image disease. CT, MRI, and ultrasound imaging are typical anatomic imaging method that can provide exact location information in the body and region of interest. anatomic imaging methods can be distinguished only by size in cm to judge disease and it is difficult to diagnose disease in an early state. Positron-emission tomography (PET), single photon emission computed tomography (SPECT) and optical imaging can detect molecular events occurring at the cellular level can be observed in the biologic process in real time and intact state, called functional imaging. So it can be applied as a tool that can archive not only early state diagnosis of disease but also characteristics of disease progression and treatment process. However functional imaging dose not provide location information. Therefore, when functional imaging is performed, position information is provided by a suitable anatomical imaging method to obtain image information.[1], [2], [3], [4]

1.2. Stimuli sensitive material and stimuli sensitive optical imaging

It is required to develop a selective delivery capability of the target

site in order to precisely visualize the target site and reduce the side effects in treating the disease. One of the methods for selective delivery to the target site has been proposed as delivery based on a stimuli-sensitive material. Stimuli-sensitive material is a substance whose physical or chemical properties are changed by external stimuli. It is changed by various stimuli. Examples are as follows; pH, enzyme, hypoxia, redox potential, and light.[5], [6], [7] Optical imaging is one of the most applied to stimuli sensitive imaging. Optical imaging has high resolution and sensitivity but is limited in use because of its high background noise.[8] To reduce noise, the fluorescence intensity should be reduced at sites other than the target site. When the fluorescent dye and quencher are close to each other, fluorescence is not expressed by förster resonance energy transfer (FRET). In the case of a cyanine dye, FRET based self-quenching can occur by the close approach of two cyanine dyes. By the FRET quenching, combining of dye and quencher using a stimuli-sensitive linker allows for selective imaging with specific stimuli at the target site. To recover fluorescence signal, enzyme,[9], [10] pH,[11] and redox condition[12] is commonly used.

1.3. Hypoxia sensitive materials

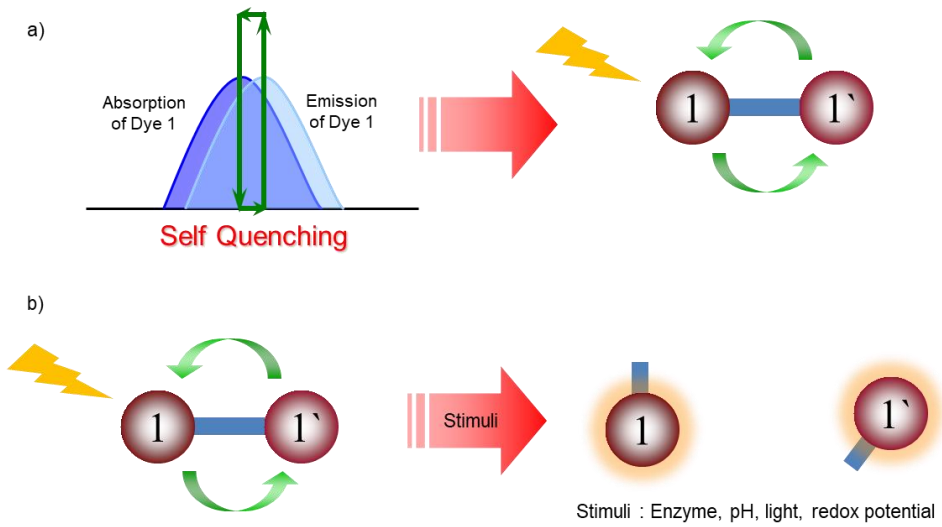

Figure 1-1. Schematic illustration of (a) FRET-based Self quenching effect and (b) Stimuli sensitive activatable imaging probe

Hypoxic condition is defined as a condition with an oxygen concentration of 1% or less and is mainly observed in conditions such as a solid tumor, stroke, and cardiac ischemia. The hypoxic condition shows higher reductive stress due to lower oxygen concentration than normal cells. As shown in Figure 1-2, nitro, azo and quinone groups are known to be reduced in the hypoxic condition to obtain amine or hydroxyl groups.[13], [14], [15], [16] Drug delivery and imaging have been studied using specific reactions in hypoxic conditions, and they are classified into two ways of releasing loaded substances. One is to release the loaded material by inducing changes in the physical properties of the delivery carrier, and the other is the chemical bond cleavage induced delivery of drugs or activatable imaging probes.

Hydrophobic nitro groups are reduced to hydrophilic amines under hypoxic conditions. These physical property changes can be applied to the selective delivery of drug delivery carriers. Hydroxylic polymers are conjugated with nitroimidazole to form polymersome[17] or self-aggregates.[18] When nitroimidazole is reduced to hydrophilic aminoimidazole under hypoxic condition, the delivery carrier becomes unstable and the release of the loaded substance is promoted. The azobenzene group is reduced in hypoxic condition to obtain two amine groups.[19], [20] Amphiphilic polymer which conjugated with a hydrophobic and hydrophilic segment by

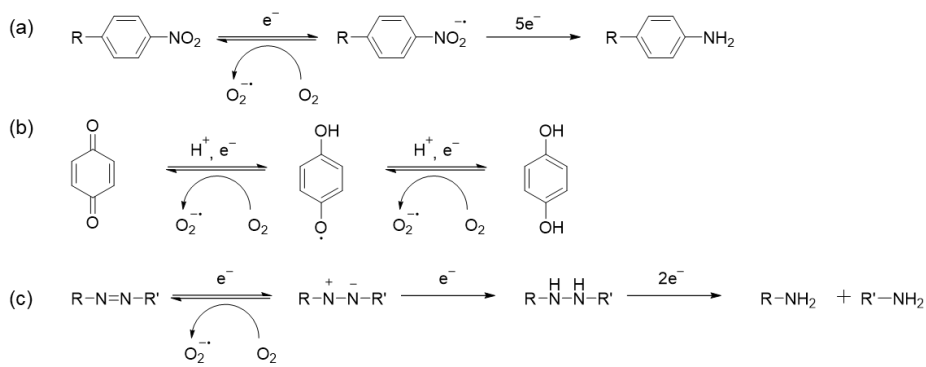

Figure 1-2. Hypoxia sensitive group (a) nitrobenzene and nitroimidazole, (b) quinone, (c) azo group

azobenzene linker form micelle that selectively degraded and release loaded drugs under hypoxic condition.[21] Also, the fluorescence dye coupled with the quencher by azo linker were separated by hypoxia and restored fluorescence and used as an imaging probe.[22], [23] When nitrobenzene is reduced to aniline, the electron density of the aromatic ring increases and the benzyl carbamate or carbonate which bonded to the ortho or para positions were degraded by act as leaving groups. This process is called 1,4-, 1,6-elimination and selective decomposition in the hypoxic condition are possible.[24] Through this process, studies have been conducted to selectively deliver a substance conjugated with a drug or imaging agent in a hypoxic condition.[15], [25], [26], [27], [28] Depending on the material structure design, multiple substances can be released rather than releasing a single substance to a single stimulus. Therefore, many studies have been conducted because it is a method of increasing the selectivity of the target site and reducing the side effects of the drug and obtaining improved imaging.[29], [30]

1.4. Self-immolative materials

Self-immolative material is a material composed of trigger, linker, and tail unit. The self-immolative material is completely decomposed by a

single stimulus to release the tail unit, mainly composed of a dendrimer and a polymer structure. It can be applied to various fields such as drug delivery, imaging probe, and biosensor since it releases multiple tail unit with one activation. The self-immolative material is degraded by the self-degradation linker which is classified as elimination-based or cyclization-based depending on the degradation process.[31] Elimination-based linkers are degraded through 1,4-elimination and 1,6-elimination. As shown in Figure 1-3, this process occurs when benzyl carbonate or benzyl carbamate is located at the ortho or para position of the masked aniline or phenol. Cyclization-based linkers are degraded by intermolecular cyclization. After the masked nucleophile is activated, it attacks the carbonyl group and induces intermolecular cyclization induced degradation. The masked nucleophile is a hydroxyl or amine group and the amine is mainly used because of its high nucleophilicity.[24], [32] Since the tail unit is degraded and released through the same process as the self-immolative linker, amine or hydroxyl group modified dye or drug is used.

The first step in the self-immolation process is the activation of the trigger. The trigger is activated through a process such as chemical reaction, enzymatic activation or light-driven activation to start cascade reaction.[33], [34], [35] As shown in Table 1, various kinds of triggers have been studied, but

there are not many triggers available in vivo condition. Nitrobenzene, azo and quinone groups can be applied as a hypoxia-sensitive trigger of self-immolative material and can be used as an imaging agent to amplify the signal by targeting hypoxic condition expressed in tumor, ischemia, etc.

1.5. Ultrasound sensitive microbubbles

Ultrasound imaging has lower resolution than CT and MRI imaging but has good accessibility to patients because of its low cost. Ultrasound imaging allows easy observation of soft tissue and blood flow, and improved images can be obtained using microbubbles or nanoemulsion as imaging agents. [36], [37] Microbubbles and nanoemulsions can play a role not only in imaging agents but also in enhancing the permeability of target sites.[38], [39], [40] When ultrasonic waves are applied to an object which can be contracted by ultrasonic waves like microbubble which is cavitated and form an acoustic wave. If the energy of the acoustic wave is sufficiently high, the cell membrane can be temporarily disrupted or the tight junction of the endothelial cell can be disturbed to increase cell permeability (Figure 1-4). In order to increase cell permeability, strong acoustic waves are required. The strong acoustic waves generated by microbubble collapse are called shock waves or

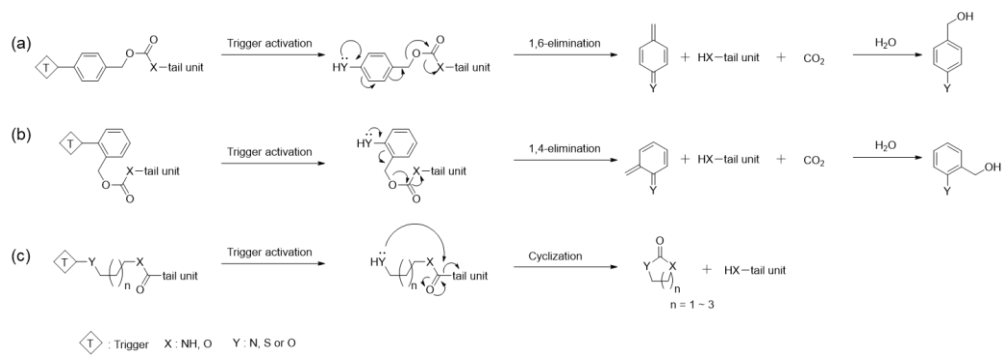

Figure 1-3. Example of self-immolative linker and basic degradation mechanism (a) 1,6-elimination, (b) 1,4-elimination, (c) Cyclization

Table 1-1. List of the trigger and their activation condition

Trigger	Activation condition
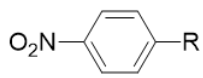	Hypoxic condition
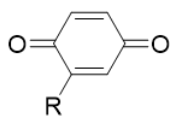	Hypoxic condition
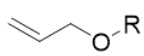	Pd / C
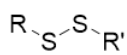	Thiol
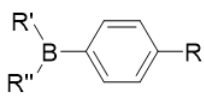	Hydrogen peroxide
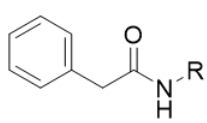	Penicillin-G-amidase (PGA)
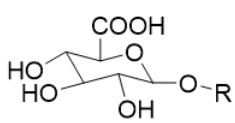	β-Glucuronidase
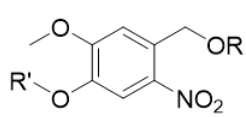	UV light

microjets. When a high-intensity ultrasound is applied to a microbubble, the strong acoustic wave generated by the collapse of the microbubble is called a shock wave or microjet. Ultrasound-induced drug delivery is possible using this phenomenon. Ultrasound-induced drug delivery is possible by delivering microbubbles to the body and ultrasound irradiation to the target site. Ultrasound-mediated delivery process can be observed in real time through ultrasound imaging and the drug delivery behavior can be assessed by labeling the fluorescent dye with the delivery carrier.

1.6. Research objective

The imaging agent which activated by specific stimuli has been spotlighted as a molecular imaging tool capable of selectively imaging the target site in the bioimaging field. Hypoxia-sensitive Self-immolative dendron is decomposed in the oxygen depletion condition and releases all of the tail units. Therefore, it is possible to selectively visualize the hypoxic condition. Microbubble selectively increases the permeability by the specific irradiation of ultrasonic to the target site, so it is possible to transfer the imaging agent or drug to the target site. In Chapter 2, hypoxia-activatable imaging probe was synthesized. A dendron was synthesized using a self-

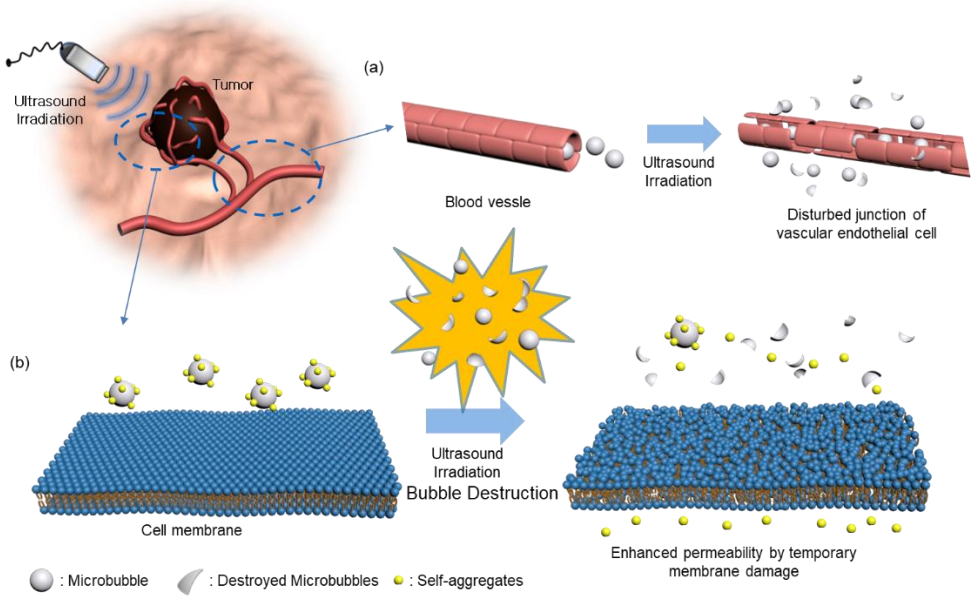

Figure 1-4. Ultrasound induced enhanced permeability at (a) blood vessel and (b) cell membrane

immolative linker, and FRET-based self-quenched Cy5.5 was conjugated as a tail unit was evaluated for selective fluorescence expression in hypoxic conditions. Tumor hypoxia levels were induced with an incubator under in vitro conditions to evaluate the potential of clinical applications by confirming the fluorescence expression ability.

In Chapter 3, we evaluated the ability of ultrasound-induced drug delivery using microbubbles. The drug delivery carrier was conjugated to the microbubble to release the drug and its stability was confirmed. The increase of permeability by ultrasound irradiation was confirmed by optical image by labeling of fluorescent dye at In vitro and In vivo conditions.

1.7. References

[1] S. S. Gambhir, Nature Reviews Cancer 2002, 2, 683.

[2] R. Weissleder, Science 2006, 312, 1168.

[3] J. K. Willmann, N. van Bruggen, L. M. Dinkelborg,S. S. Gambhir, Nature Reviews Drug Discovery 2008, 7, 591.

[4] S. Y. Lee, S. I. Jeon, S. Jung, I. J. Chung,C.-H. Ahn, Advanced Drug Delivery Reviews 2014, 76, 60.

[5] M. Wei, Y. Gao, X. Li,M. J. Serpe, Polymer Chemistry 2017, 8, 127.

[6] S. Ganta, H. Devalapally, A. Shahiwala,M. Amiji, Journal of Controlled Release 2008, 126, 187.

[7] S. Mura, J. Nicolas,P. Couvreur, Nature Materials 2013, 12, 991.

[8] J. Zhao, G. Jin, G. Weng, J. Li, J. Zhu,J. Zhao, Drug Discovery Today 2017, 22, 1367.

[9] V. Ntziachristos, C.-H. Tung, C. Bremer,R. Weissleder, Nature Medicine 2002, 8, 757.

[10] J. H. Ryu, A. Lee, J. H. Na, S. Lee, H. J. Ahn, J. W. Park, C.-H. Ahn, B.-S. Kim, I. C. Kwon, K. Choi, I. Youn,K. Kim, Amino Acids 2011, 41, 1113.

[11] A. K. Galande, R. Weissleder,C.-H. Tung, Bioconjugate Chemistry 2006, 17, 255.

[12] M. Tsuji, S. Ueda, T. Hirayama, K. Okuda, Y. Sakaguchi, A. Isono,H. Nagasawa, Organic & Biomolecular Chemistry 2013, 11, 3030.

[13] K. A. Krohn, J. M. Link,R. P. Mason, Journal of nuclear medicine : official publication, Society of Nuclear Medicine 2008, 49 Suppl 2, 129s.

[14] K. Kiyose, K. Hanaoka, D. Oushiki, T. Nakamura, M. Kajimura, M. Suematsu, H. Nishimatsu, T. Yamane, T. Terai, Y. Hirata,T. Nagano, Journal of the American Chemical Society 2010, 132, 15846.

[15] L. Cui, Y. Zhong, W. Zhu, Y. Xu, Q. Du, X. Wang, X. Qian,Y. Xiao, Organic Letters 2011, 13, 928.

[16] N. El-Najjar, H. Gali-Muhtasib, R. A. Ketola, P. Vuorela, A. Urtti,H. Vuorela, Phytochemistry Reviews 2011, 10, 353.

[17] J. Yu, C. Qian, Y. Zhang, Z. Cui, Y. Zhu, Q. Shen, F. S. Ligler, J. B. Buse,Z. Gu, Nano Letters 2017, 17, 733.

[18] T. Thambi, V. G. Deepagan, H. Y. Yoon, H. S. Han, S.-H. Kim, S. Son, D.-G. Jo, C.-H. Ahn, Y. D. Suh, K. Kim, I. Chan Kwon, D. S. Lee,J. H. Park, Biomaterials 2014, 35, 1735.

[19] J. Yu, Y. Zhang, X. Hu, G. Wright,Z. Gu, Annals of Biomedical Engineering 2016, 44, 1931.

[20] S. Zbaida,W. G. Levine, Chemical Research in Toxicology 1991, 4, 82.

[21] P. Kulkarni, M. K. Haldar, P. Katti, C. Dawes, S. You, Y. Choi,S. Mallik, Bioconjugate Chemistry 2016, 27, 1830.

[22] W. Piao, S. Tsuda, Y. Tanaka, S. Maeda, F. Liu, S. Takahashi, Y. Kushida, T. Komatsu, T. Ueno, T. Terai, T. Nakazawa, M. Uchiyama, K. Morokuma, T. Nagano,K. Hanaoka, Angewandte Chemie International Edition 2013, 52, 13028.

[23] Q. Cai, T. Yu, W. Zhu, Y. Xu,X. Qian, Chemical Communications 2015, 51, 14739.

[24] A. Alouane, R. Labruère, T. Le Saux, F. Schmidt,L. Jullien, Angewandte Chemie International Edition 2015, 54, 7492.

[25] R. Madec-Lougerstay, J.-C. Florent,C. Monneret, Journal of the Chemical Society, Perkin Transactions 1 1999, 1369.

[26] P. L. Carl, P. K. Chakravarty,J. A. Katzenellenbogen, Journal of Medicinal Chemistry 1981, 24, 479.

[27] W. A. Denny, Future Oncology 2010, 6, 419.

[28] T. Guo, L. Cui, J. Shen, W. Zhu, Y. Xu,X. Qian, Chemical Communications 2013, 49, 10820.

[29] R. J. Amir, N. Pessah, M. Shamis,D. Shabat, Angewandte Chemie International Edition 2003, 42, 4494.

[30] F. M. H. de Groot, C. Albrecht, R. Koekkoek, P. H. Beusker,H. W. Scheeren, Angewandte Chemie International Edition 2003, 42, 4490.

[31] I. Tranoy-Opalinski, A. Fernandes, M. Thomas, J. P. Gesson,S. Papot, Anti-cancer agents in medicinal chemistry 2008, 8, 618.

[32] Y. Ge, X. Wu, D. Zhang,L. Hu, Bioorganic & Medicinal Chemistry Letters 2009, 19, 941.

[33] A. D. Wong, M. A. DeWit,E. R. Gillies, Advanced Drug Delivery Reviews 2012, 64, 1031.

[34] M. E. Roth, O. Green, S. Gnaim,D. Shabat, Chemical Reviews 2016, 116, 1309.

[35] R. E. Wang, F. Costanza, Y. Niu, H. Wu, Y. Hu, W. Hang, Y. Sun,J. Cai, Journal of Controlled Release 2012, 159, 154.

[36] E. G. Schutt, D. H. Klein, R. M. Mattrey,J. G. Riess, Angewandte Chemie International Edition 2003, 42, 3218.

[37] A. L. Klibanov, P. T. Rasche, M. S. Hughes, J. K. Wojdyla, K. P. Galen, J. H. J. Wible,G. H. Brandenburger, Investigative Radiology 2004, 39, 187.

[38] N. Y. Rapoport, A. M. Kennedy, J. E. Shea, C. L. Scaife,K.-H. Nam, Journal of Controlled Release 2009, 138, 268.

[39] K. Ferrara, R. Pollard,M. Borden, Annual Review of Biomedical

Engineering 2007, 9, 415.

[40] H.-L. Liu, C.-H. Fan, C.-Y. Ting,C.-K. Yeh, Theranostics 2014, 4, 432.

Chapter 2.

Development of Hypoxia-Activatable Optical Imaging Probe

2.1. Introduction

Unlike normal cells where a continuous and adequate amount of oxygen is supplied through the blood vessels, the tumor shows hypoxic conditions due to a poor oxygen supply. Hypoxia is generally defined as an environment with less than 2 % oxygen level [1], [2] and is expressed in environments such as ischemia[3], and solid tumors[4]. This is indicated by the perfusion limit due to abnormal angiogenesis and the diffusion limit due to the limit in oxygen diffusion. The hypoxic condition produces hypoxia-inducible factor 1 (HIF-1) which helps to resist hypoxic conditions and have increased reductive stress. This specific environment has the potential to be useful for tumor imaging and therapy. Various studies have been actively carried out for the use of prodrug using nitro group,[5], [6] quinone,[7], [8] azo group,[9] etc. In case of solid tumors, the imaging agent is difficult to access because it is difficult to supply blood to core of solid tumor and the hypoxic condition is generally expressed in the center of tumor.[10]

Dendrimer has well defined 3-D branched structure with multiple end groups. It has nanoscopic size, narrow polydispersity index and available to change its property by modifying multiple end groups. Due to its unique properties, Dendrimer has wide potential applications; catalysis, liquid crystal,

sensors, and biomedical applications and so on. The application of dendrimer in the biomedical field is currently drawing a lot of scientific attention.[11], [12], [13] In this experiment, we propose a hypoxic sensitive dendrimer structure that has the ability to easily access to the solid tumor because of its nanoscopic size.

Releasing molecules which conjugated with dendrimer end group from a dendrimer by degradation triggered by single stimuli is proposed by several groups with the following names, cascade-release dendrimers, dendrimers disassembly or self-immolative dendrimers[14], [15], [16], [17]. Because multiple releases of molecules with a single stimulus, it has been widely studied to apply drug delivery and imaging. In generally, self-immolative dendrimer has the following structure. Nitro, quinone and azo group were used to apply stimuli sensitive trigger, and carbonate or carbamate linker is used as a linker to constitute a dendrimer structure.[18], [19], [20], [21] Nitro group is reduced to aniline under hypoxic condition by nitroreductase.[2], [22], [23] In the presence of benzyl carbonate or benzyl carbamate at the ortho or para position of the resulting aniline, degradation occurs through 1,4- and 1,6-elimination reactions.[24], [25] This allows the design of a self-immolative dendrimer and the synthesis of hypoxia-activatable optical imaging probes through the introduction of fluorescent dye at the end group of the dendrimer.

In the case of fluorescent materials, Förster resonance energy transfer (FRET) based quenching is possible when donor and acceptor approaches within 10 nm.[26], [27] If the stoke shift of the fluorescent material is sufficiently small, the absorbance and the emission overlap each other. When fluorescent dyes are in close proximity to each other, self-quenching occurs because dye could act as both donor and acceptor. Cy5.5 is a representative self-quenching dye, and when Cy5.5 is conjugated to the dendrimer end, FRET-based self-quenching occurs due to the small size of the dendrimer and a short distance between the dendrimer end groups. In addition, when the dendrimer is selectively degraded in the hypoxic condition, the conjugated Cy5.5 is released and the fluorescence can be recovered. Selective fluorescence expression provides a high signal-to-noise level that is important in fluorescence imaging, thereby providing effective fluorescence imaging capabilities[28].

In this study, we synthesize a self-immolative dendrimer to apply fluorescence imaging probe. Dendrimers are expected to display advantages in accessing the hypoxic region based on the relatively small hydrodynamic volumes. Nitro group was applied at the core of dendrimers to provide a modification site which showed structural changes with hypoxia sensitivity. After the nitro group was reduced in hypoxic condition, self-immolative

reaction was sequentially progressed through carbamate linkage. Such changes resulted in the release of FRET-quenched fluorescence dyes conjugated at the periphery of dendritic building blocks and produced a hypoxia-sensitive fluorescence imaging probe.

2.2. Experimental

Materials. 2,4-dimethyl-1-nitrobenzene (98 %), 4-nitrobenzyl alcohol (NB, 98 %) and 4-nitrophenyl chloroformate (NPC, 98 %) were commercially available from Tokyo Chemical Industry Co., Ltd. (Japan).

Potassium permanganate ($KMnO_4$, 99 %), triethyl amine (TEA, 99 %), N,N-dimethylformamide (DMF, anhydrous, 99.8 %), Methanol (MeOH, anhydrous, 99.8 %), Zinc powder (Zn), acetic acid (AcOH, 99.7 %), lithium aluminum hydride ($LiAlH_4$, 95 %) and pyridine (99.0 %) were purchased from Sigma-Aldrich (St. Louis, MO, USA). 1-Hydroxybenzotriazole hydrate (HOBt, anhydrous) was obtained from AnaSpec, Inc (Fremont, CA, USA). Sulfuric acid (H_2SO_4, 98 %), magnesium sulfate ($MgSO_4$, 99 %), dichloromethane (MC, 99 %), Sodium hydroxide (NaOH, 97 %), sodium chloride (NaCl, 99 %), sodium bicarbonate ($NaHCO_3$, 99~100.5%), ethyl acetate (EtOAc, 99.5 %) and tetrahydrofuran (THF, 99.5 %) were obtained from daejung chemicals and Metals Co. (Korea). Flamma 675 amine (Cy5.5) was purchased from BioActs (Korea). Silica gel 60 (70~230 mesh) for column chromatography was purchased from Merck & Co. (Germany). THF was distilled from sodium benzophenone, MC, pyridine, and TEA were dried over calcium hydride and all other chemicals were used

as received without further purification. Water was double distilled before use.

Instruments. ^{1}H-NMR analysis was performed using Bruker Avance 300 MHz spectrometer in $CDCl_3$ or DMSO-d_6 at room temperature. UV-vis spectra were recorded from UV-2450 by Shimadzu (Tokyo, Japan) scanned over the range of 550~800 nm. Fluorescence emission spectra were obtained by a Photo Technology International, Felix32 QM-40 (Kyoto, Japan). The hypoxic condition was maintained using a CO_2/O_2 incubator (Vision Scientific Co., Ltd, Korea). Confocal microscopy image was obtained by IX81-ZDC focus drift compensating microscope (Olympus, Tokyo, Japan)

2.3.1 4-nitroisophthalic acid (B2). In 500 mL 2-neck round bottom flask, 2,4-dimethyl-1-nitrobenzene (B1) (11.3 g, 74.8 mmol) was dispersed in water (200 mL), followed by portionwise addition of $KMnO_4$ (29.5 g, 186.0 mmol). After the addition was complete, the reaction mixture was heated to reflux with stirring for 24 h. The reaction mixture was filtered through celite and the filtrate was collected. The filtrate was acidified with concentrated HCl, extracted with EA (3 x 100 mL), and the organic layer was collected. The organic layer was dried over $MgSO_4$ and evaporated in vacuo. The resulting powder was resuspended in $CHCl_3$ (600 mL) followed by sonication for 1 h.

The suspension was filtered to give white solid (6.5 g, 40 %).

^{1}H-NMR spectrometer are as follows. (300 MHz, $CDCl_3$): δ 8.31 (s, 1H, Ar*H*), 8.25 (d, *J* = 8.3, 1H, Ar*H*), 8.505 (d, *J* = 8.3, 1H, Ar*H*)

2.3.2 dimethyl 4-nitroisophthalate (B3). 75 mL methanol dissolving (B2) (6.0 g, 28.3 mmol) was charged to a 2-neck round bottom flask. 98 % H_2SO_4 solution (3.8 mL) was slowly put into the flask and the reaction mixture was heated to reflux for 12 h under nitrogen atmosphere. After the reaction, the reaction mixture was evaporated in vacuo and dissolved in EA (100 mL). The reaction mixture was extracted by saturated NaCl solution (100 mL) and saturated $NaHCO_3$ solution (2 x 100 mL). The organic layer was dried over $MgSO_4$ and evaporated in vacuo to give (B2) as a white solid (5.7 g, 83 %)

^{1}H-NMR spectrometer are as follows. (300 MHz, $CDCl_3$): δ 8.44 (s, 1H, Ar*H*), 8.29 (d, *J* = 8.3, 1H, Ar*H*), 7.93 (d, *J* = 8.3, 1H, Ar*H*), 3.98 (d, *J* = 11.6, 6H, CH_3OCO-)

2.3.3 dimethyl 4-aminoisophthalate (B4). A mixture of (B3) (6.0 g, 25.1 mmol), Zn powder (6.0 g, 91.8 mmol) in a mixture of MC (50 mL) and methanol (60 mL) was introduced into a 250 mL 2-neck round bottom flask

equipped with a reflux condenser and dropping funnel. The reaction mixture was heated under reflux condition under nitrogen atmosphere, followed by dropwise of acetic acid (6 mL, 104 mmol) in methanol (40 mL) within 30 min and stirring for 4 h. The solids were removed by filtration and the filtrate was evaporated in vacuo. The residue was dissolved in MC (100 mL) and extracted with saturated $NaHCO_3$ solution (2 x 100 mL). The organic layers were dried over $MgSO_4$, and the solvent was evaporated to give white solid (4.2 g, 80 %).

^{1}H-NMR spectrometer are as follows. (300 MHz, $CDCl_3$): δ 8.59s, 1H, Ar*H*), 7.92 (d, *J* = 8.8, 1H, Ar*H*), 6.65 (d, *J* = 8.7, 1H, Ar*H*), 6.10 (br s, 2H, -NH_2), 3.89 (d, *J* = 7.3, 6H, CH_3OCO-)

2.3.4 (4-amino-1,3-phenylene)dimethanol (Building block). $LiAlH_4$ (1.1 g, 30.6 mmol) was introduced into nitrogen charged 250 mL 2-neck round bottom flask equipped with a dropping funnel. THF (60 mL) was added under an ice bath, followed by dropwise addition of (B3) (4.0 g, 19.1 mmol) in THF (40 mL) within 30 min. The resulting mixture was stirred at room temperature for 4 h. After resulting mixture was cooled to 0 °C, $LiAlH_4$ was quenched by successive addition of H_2O (1.1 mL), 15 % NaOH (1.1 mL) and H_2O (3.3 mL). The resulting slurry was filtered through celite and

filtrated was collected. After removing the volatiles in vacuo, the residue was dissolved in minimum amount of THF. The white solid was isolated by precipitating into ice-cold MC (200 mL). (1.7 g, 57 %)

^{1}H-NMR spectrometer are as follows. (DMSO, ppm): δ 7.00 (s, 1H, Ar*H*), 6.89 (d, *J* = 8.2, 1H, Ar*H*), 6.55 (d, *J* = 8.0, 1H, Ar*H*), 4.95 (t, *J* = 8.9, 2H, -NH_2), 4.80 (s, 2H, -OH), 4.78 (dd, *J* = 33.4, 8.8, 4H, ArCH2O-)

2.3.5 4-nitrobenzyl (4-nitrophenyl) carbonate (NB-Act). In 100 mL 2-neck round bottom flask, 4-nitrobenzyl alcohol (5.0 g, 32.7 mmol) was dissolved in MC (50 mL). NPC (7.9 g, 39.2 mmol) and TEA (5.5 mL, 39.2 mmol) were successively added. The mixture was stirred at room temperature for 12 h under nitrogen atmosphere. After the reaction, the reaction mixture was extracted by saturated NaCl solution (3 x 200 mL), double distilled water (2 x 200 mL) and the organic layer was dried over $MgSO_4$. After removing the volatiles in vacuo, the residue was crystallized from EA/hexane affording as a pale yellow solid (8 g, 76 %).

^{1}H-NMR spectrometer are as follows. (DMSO, ppm): δ 8.30 (q, *J* = 13.7, 8.4, 4H, Ar*H*), 7.67 (dd, *J* = 43.8, 8.4, 4H, Ar*H*), 5.46 (s, 2H, ArCH_2O-), 4.95 (t, *J* = 8.9, 2H, -NH_2), 4.80 (s, 2H, -OH), 4.78 (dd, *J* = 33.4, 8.8, 4H, ArCH2O-)

2.3.6 4-nitrobenzyl (2,4-bis(hydroxymethyl)phenyl)carbamate (G0). (NB-Act) (2.5 g, 7.9 mmol), HOBt (1.4 g, 9.4 mmol) and DMF (25 mL) were put into 100 mL 2-neck round bottom flask under nitrogen atmosphere. (Building block) (1.4 g, 9.4 mmol) in 10 mL DMF was put into 2-neck round bottom flask. The reaction mixture was heated at 40 °C and stirred for 16 h. After the reaction, the reaction mixture was precipitated in 300 mL methanol and purified by column chromatography (EA) to give (G0) as a white solid (1.3 g, 50 %).

^{1}H-NMR spectrometer are as follows. (DMSO, ppm): δ 8.99 (s, 1H, CONH), 8.25 (d, *J* = 8.6, 2H, Ar*H*), 7.67 (d, *J* = 8.6, 2H, ArH), 7.42 (d, *J* = 8.0, 1H, ArH), 7.33 (s, 1H, ArH), 7.16 (d, *J* = 8.5, 1H, ArH), 5.33 (t, *J* = 5.3, 1H, OH), 5.27 (s, 2H, ArCH2OCO), 5.11 (t, *J* = 5.7, 1H, OH), 4.48 (dd, *J* = 19.5, 5.5, 4H, ArCH2O)

2.3.7 4-nitrobenzyl (2,4-bis((((4-nitrophenoxy)carbonyl)oxy) methyl)phenyl)carbamate (G0-Act). (G0) (2.0 g, 6.0 mmol), NPC (3.6 g, 18.1 mmol) and THF (150 mL) were charged into a 500 mL 2-neck round bottom flask which placed in an ice bath under nitrogen atmosphere. Pyridine (1.45 mL, 18.06 mmol) was added to reaction mixture, the temperature was raised up to room temperature and stirred for 24 h. After the reaction, 200 mL

of MC was poured into the reaction mixture and solution was extracted by saturated NaCl solution (3 x 200 mL) and the organic layer was dried over $MgSO_4$. After removing the volatiles in vacuo, the residue was crystallized from EA/hexane affording as a white solid (2.4 g, 60 %).

^{1}H-NMR spectrometer are as follows. (DMSO, ppm): δ 8.30 (m, 4H), 8.10 (d, *J* = 9.15, 2H), 7.73 (m, 3H), 7.55 (dd, *J* = 12.9, 8.7, 4H), 6.91 (d, *J* = 9.2, 2H), 5.41 (m, 6H)

2.3.8 4-nitrobenzyl (2,4-bis((((2,4-bis(hydroxymethyl)phenyl) carbamoyl)oxy)methyl)phenyl)carbamate (G1). (G0-Act) (2.0 g, 3.0 mmol), HOBt (1.1 g, 7.3 mmol) and DMF 10 mL were transferred into 100 mL 2-neck round bottom flask under nitrogen atmosphere. Building block (1.1 g, 7.3 mmol), dissolved in 10 mL DMF, was added into the reaction mixture. The temperature was raised up to 40 °C and the reaction mixture was kept for 24 h under continuous stirring. The reaction medium was cooled down to room temperature and precipitated in 200 mL water to obtain powder. The residue was purified by column chromatography (EA/THF 3/1) to give (G1) as a white solid (1.3 g, 50 %).

^{1}H-NMR spectrometer are as follows. (DMSO, ppm): δ 9.39 (s, 1H), 8.86 (d, *J* = 11.7, 2H), 8.23 (d, *J* = 8.6, 2H), 7.67 (d, *J* = 8.5, 2H), 7.45 (m,

5H), 7.31 (s, 2H), 7.14 (d, *J* = 8.0, 2H), 5.32 (br s, 4H), 5.12 (m, 6H), 4.46 (dd, *J* = 16.7, 5.4, 4H)

2.3.9 4-nitrobenzyl (2,4-bis((((2,4-bis((((4-nitrophenoxy)carbonyl) oxy)methyl)phenyl) carbamoyl)oxy)methyl)phenyl)carbamate (G1-Act). In a 500 mL 2-neck round bottom flask, (G1) (1.3 g, 2.3 mmol) and NPC (2.3 g, 11.3 mmol) were dissolved in 150 mL THF which placed in an ice bath under nitrogen atmosphere. Pyridine (0.9 mL, 11.3 mmol) was added into the flask and the reaction mixture warmed up to 40 °C for 12 h under continuous stirring. 150 mL MC was transferred to the flask and the reaction mixture was reacted with reflux for an additional 12 h. After the reaction media was cooled down to room temperature, solvents were removed in vacuo and redissolved in 200 mL MC. The organic layer was extracted with saturated NaCl solution (3 x 150 mL), distilled water (150 mL) and the organic layer was dried over $MgSO_4$. After removing the volatiles in vacuo, the residue was crystallized from EA/hexane affording as a white solid (1.4 g, 55 %).

^{1}H-NMR spectrometer are as follows. (DMSO, ppm): δ 9.36 (s, 2H), 8.26 (m, 8H), 8.10 (d, *J* = 9.2, 2H), 7.68-7.42 (m, 17H), 6.90 (d, *J* = 9.0, 2H), 5.37-5.14 (m, 14H)

2.3.10 Synthesis of Cy5.5 conjugated dendron (G1-Cy5.5). In a 10 mL Schlenk flask, (G1-Act) (5.0 mg, 3.7 μmol), Cy5.5 (20.0 mg, 18 μmol) and TEA (2.0 mg, 18 μmol) were dissolved in DMF under nitrogen atmosphere. The reaction was kept in dark condition for 12 h with stirring. The resulting solution was transferred to a dialysis bag (MWCO : 1,000) and dialyzed against deionized water for 24 h to remove the organic solvents and free Cy5.5, followed by lyophilized to give (G1-Cy5.5) as a blue powder (16.8 mg, 84 %)

^{1}H-NMR spectrometer are as follows. (DMSO, ppm): δ 9.00 (s, 8H), 8.44 (s, 16H), 8.22 (s, 8H), 7.81-7.65 (m, 13H), 7.50-7.22 (m, 14 H), 6.67-6.62 (m, 4H), 6.43-6.31 (m, 8H), 5.27-4.93 (m, 14H), 3.03 (m, 16H), 1.95 (s, 40H), 1.32-1.23 (m, 48H)

Cascade-degradation and fluorescence recovery in hypoxic condition. 100 mM NADPH in 10 mL PBS buffer was degassed by N_2 bubbling for 2 h and the reaction mixture was heated at 37 °C. G1-Cy5.5 (0.13 mg, 0.023 μmol) was added to the degassed reaction mixture and react in dark condition for 12 h. After the reaction, fluorescence emission spectra were obtained by a Photo Technology International, Felix32 QM-40. The excitation wavelength was 620 nm (excitation slit width = 10 mm, emission slit width =

5 mm), the emission wavelength was recorded over the range of 640~800 nm.

In vitro fluorescence recovery in hypoxic condition. SCC7 cells were cultured in RPMI 1640 with 10 % FBS and 1 % penicillin-streptomycin. Cells were maintained at 37 °C in a humidified 5% CO_2 - 95% air atmosphere. The cells were seed at a concentration of 1 x 10^4 cells/well in flat-bottomed plates and allowed to grow overnight at 37 °C. To measure the fluorescence recovery of (G1-Cy5.5), cells treated with (G1-Cy5.5) were incubated at hypoxic or normoxic conditions for a predetermined time interval. After incubation, the cells were washed with PBS and fixed with 4 % formaldehyde solution. For nuclear staining, the cell was incubated with DAPI (4,6-diamino-2-phenylindole) for 10 min at RT, followed by washing with PBS. The intracellular localization of Cy5.5 released from (G1-Cy5.5) was monitored using IX81-ZDC focus drift compensating microscope (Olympus, Tokyo, Japan)

2.3. Results and discussion

The synthesis of hypoxia sensitive dendrimer was achieved as depicted in Scheme 2-1 and 2-2. In this experiment, a hypoxia-activatable optical probe was synthesized using 4-nitrobenzyl alcohol (NB) as a starting material. Dendrimer building block was synthesized using (B1) and the products were confirmed by ^{1}H-NMR and UV-Vis spectroscopy. 2,4-dimethyl-1-nitrobenzene (B1), benzyl carbon is oxidized by $KMnO_4$ to form a dicarboxylic acid group, which is esterified by reacting with methanol under H_2SO_4 catalyst. The nitro group was reduced to aniline by Zn-HCl and finally the ester group was reduced to alcohol by $LiAlH_4$ to obtain a dendron building block which has two benzyl alcohol and aniline. Hypoxia-activatable optical probe was synthesized through the conjugation of building blocks and Cy5.5 after activation of benzyl alcohol (NB) with 4-nitrophenyl chloroformate (NPC).

Dendron synthesis was performed using NPC activation chemistry. The nitrophenyl group, which is formed by the reaction of NPC and alcohol, is a good leaving group so it reacts easily with nucleophiles and widely used for conjugation with other substances. In the dendron growth process, HOBt was used as a coupling agent.[19] HOBt increases the reactivity of NPC-

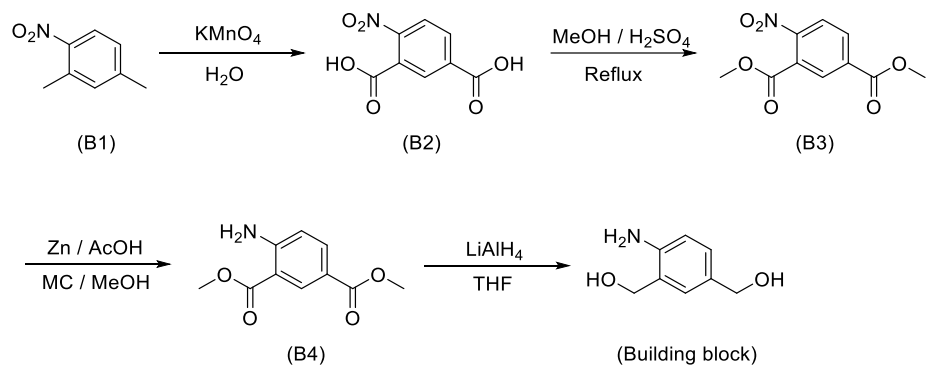

Scheme 2-1. Schematic scheme of (Building block)

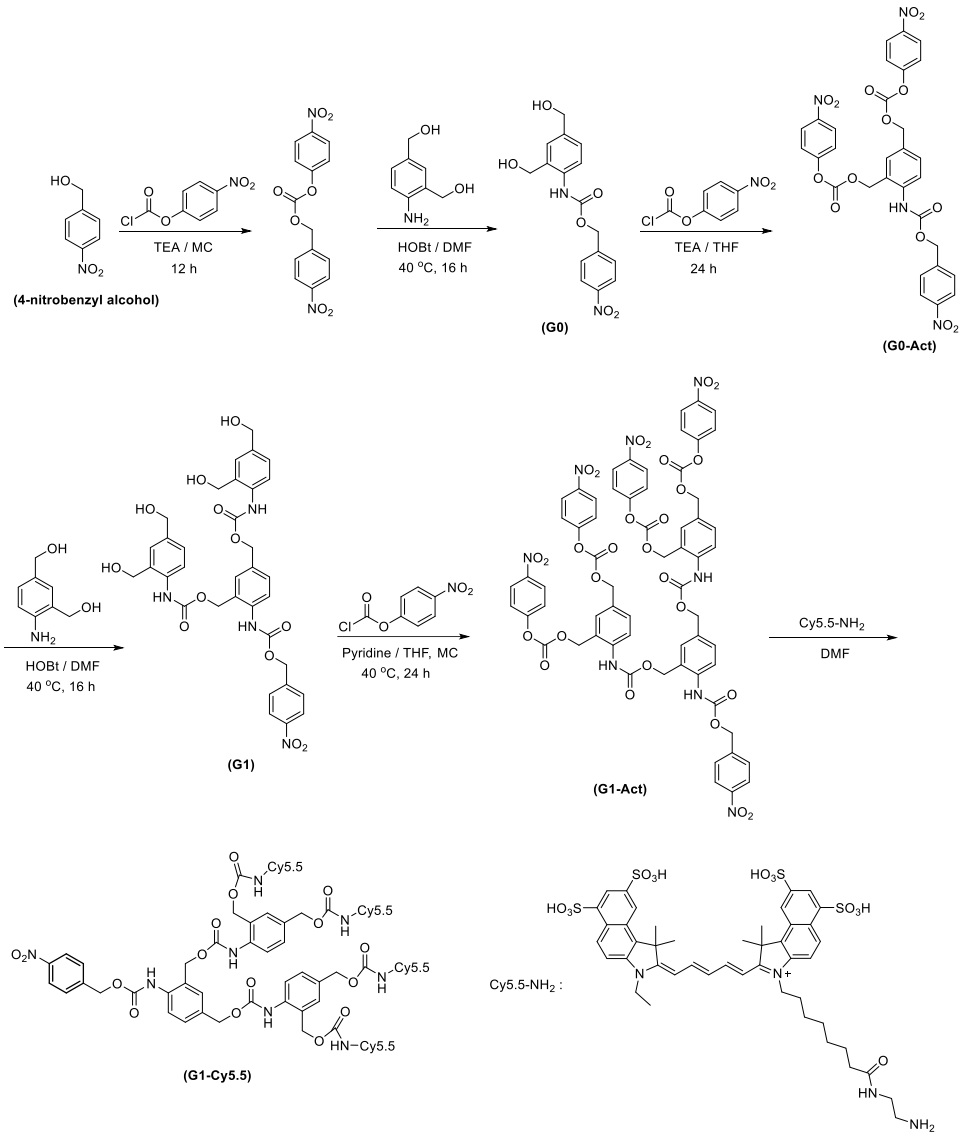

Scheme 2-2. Schematic scheme of (G1-Cy5.5)

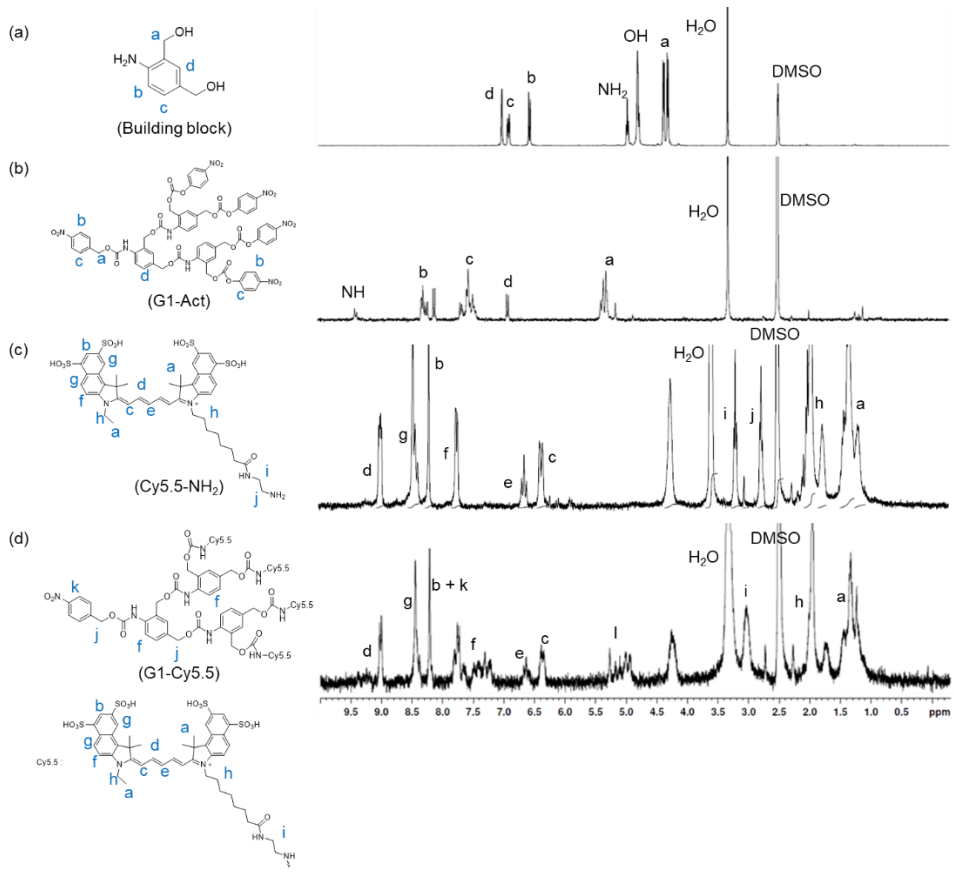

Figure 2-1. ^{1}H NMR spectra of (Building block), (G1-Act), (Cy5.5), and (G1-Cy5.5)

activated benzyl alcohol, allow to react relatively less reactive aniline. Aniline has lower nucleophilicity than primary amines but aniline is more reactive than benzyl alcohol. Therefore, carbonate form product was not obtained and only carbamate form product was obtained. Finally, (G1-Cy5.5) was synthesized by reacting NPC-activated (G1-Act) with amine functionalized Cy5.5 and the degree of functionalization was around 100 % when confirmed by ^{1}H-NMR (Figure 2-2 (d)). As depicted in Figure 2-3, (G1-Cy5.5) could be confirmed that the UV absorbance peak shape was changed in comparison with Cy5.5. Cy5.5 form dimer or H-, J-aggregate when they were close to each other. It is known that the UV absorbance pattern changes in this case.[29], [30], [31] Since Cy5.5 which was conjugated at the periphery of dendron, it is thought to exist as a dimer form by a short distance between the dendron end group.

We hypothesized that the nitro group of (G1-Cy5.5) is reduced by nitroreductase in hypoxic condition and hypoxia sensitive degradation occurs. Nitro group is known to be reduced to aniline by nitroreductase in hypoxic condition.[32], [33] NADPH is one of the representative nitroreductases. Nitro groups are reduced by obtaining electrons by nitroreductase in hypoxic condition. However, in the normoxic condition, the oxygen present in the surroundings deprives the electrons of the nitro group and maintains the nitro

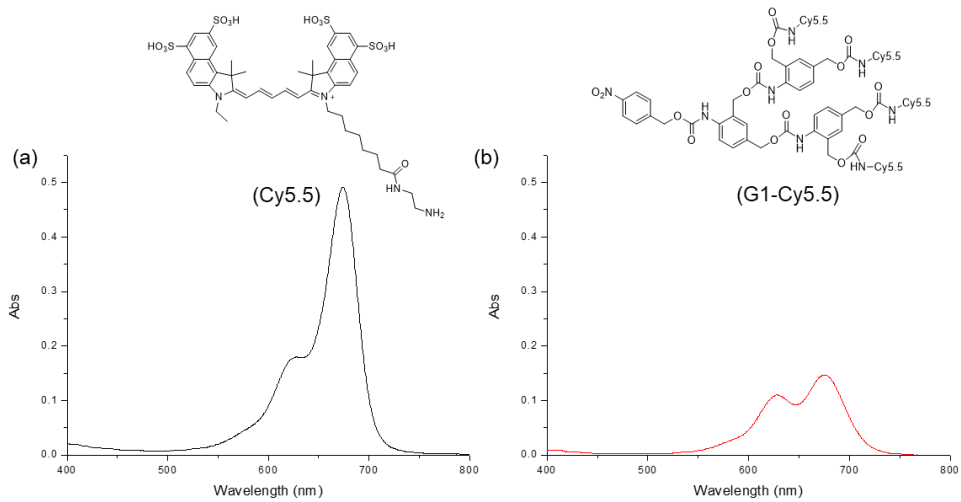

Figure 2-2. UV absorbance spectra of (a) (Cy5.5) and (b) (G1-Cy5.5)

group form. When the nitro group was reduced and reduced to aniline under hypoxic condition, the carbamate group which is the linker of the dendron, was decomposed by electron density change of the aromatic ring. Decomposition proceeds through a 1,4-and 1,6-elimination reaction process in which benzyl carbonate acts as a leaving group. [33], [34], [35] Through this process, the dendron is cascade degraded and the release of Cy5.5, which was conjugated to the dendron end by a single trigger event. As shown in Figure 2-4, it was confirmed that the fluorescence recovery of Cy5.5 which triggered by a degradation of (G1-Cy5.5) by NADPH in hypoxic condition. (G1-Cy5.5) incubated in Hypoxic condition showed fluorescence intensity about 20 times higher than that of untreated (G1-Cy5.5). Since (G1-Cy5.5) has a high signal-to-noise value, it can provide a more accurate fluorescence image when used as a hypoxia-activatable imaging probe.

To confirm the fluorescence recovery ability of (G1-Cy5.5) at in vitro condition, SCC-7 cells were incubated to hypoxic conditions in an incubator to observe fluorescence signal changes. (G1-Cy5.5) were transferred to SCC-7 cell in culture media and incubate in hypoxic condition (1 % O_2, 5 % CO_2) and normoxic condition (20 % O_2, 5 %). As depicted in figure 2-5, when SCC7 cells were incubated in hypoxic condition, it was confirmed that the fluorescence recovery begins after about 6 h. However, it could be seen that

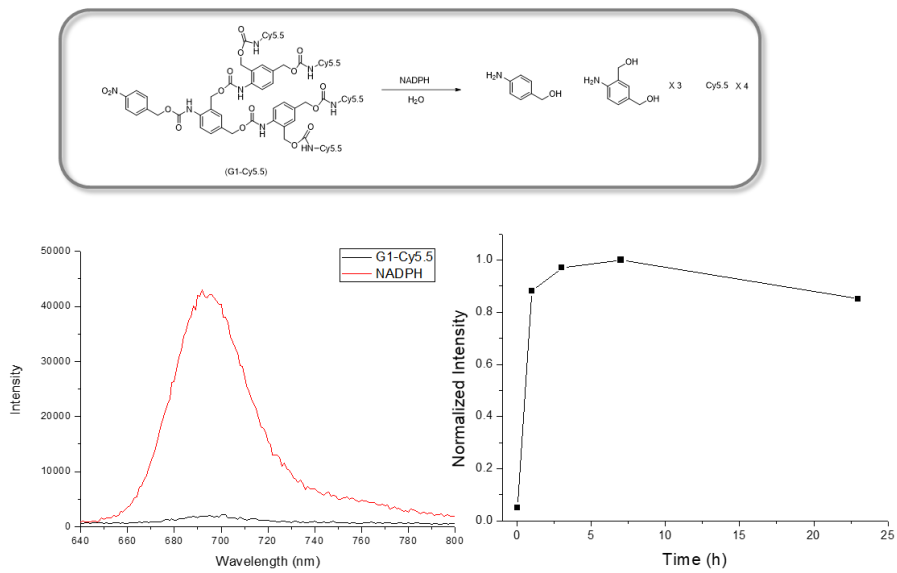

Figure 2-3. Fluorescence (λEx = 620 nm, λEm = 640 ~ 800 nm) emitted upon incubation of G1-Cy5.5 in hypoxic or normoxic condition

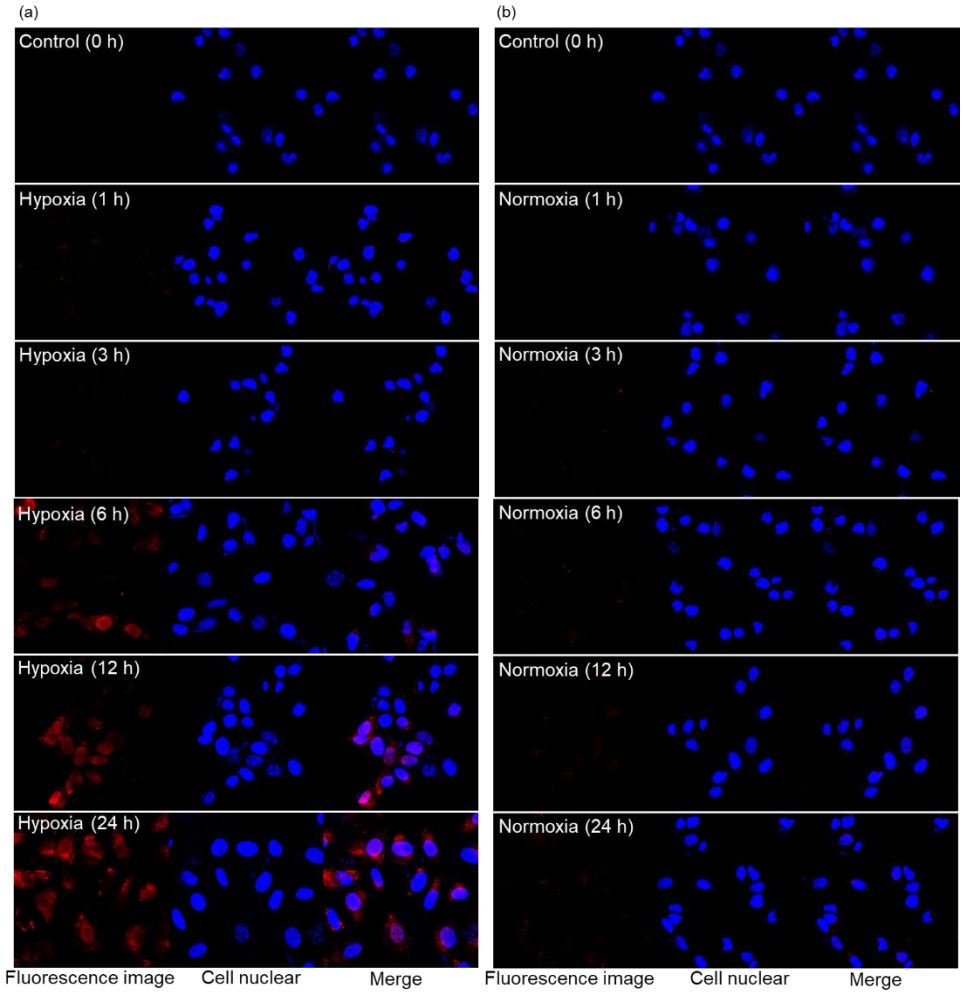

Figure 2-4. Confocal microscopy image of SCC-7 cell which treat with G1-Cy5.5 in (a) hypoxic condition and (b) normoxic condition

fluorescence recovery was rarely observed in the normoxic condition. This suggests that G1-Cy5.5 is selectively degraded in hypoxic condition, releasing Cy5.5, and it was confirmed that the nitro group is successfully reduced by nitroreductase presence in the cell environment. The hypoxia-induced In vitro degradation rate of G1-Cy5.5 show slower than N_2 bubbling condition with NADPH. This suggests that it takes time to reach the hypoxic condition of the cell culture medium in the hypoxic chamber and due to the relatively high oxygen concentration compared to the N_2 bubbling.

2.4. Conclusion

In this research, we successfully synthesized an activatable optical probe G1-Cy5.5 which selectively degraded in the hypoxic condition and displays fluorescence. We synthesized G1-Cy5.5 using the nitro group as a hypoxia sensitive trigger and carbamate as a linker. Cy5.5 which conjugated to the dendrimer end group was released by reduction of the nitro group by nitroreductase under hypoxic conditions. The recovered fluorescence signal shows 20 times higher intensity than G1-Cy5.5. Because of high signal-to-noise level, G1-Cy5.5 is expected to show high performance of activatable imaging probe. Also, the selective fluorescence signal was expressed when

the hypoxic condition was induced in vitro condition. Hypoxia-activatable optical imaging probes were synthesized through this study and we suggested that activatable imaging probe have possibility of selective imaging of hypoxic tumor sites in vivo.

2.5. References

[1] J. M. Brown,W. R. Wilson, Nature Reviews Cancer 2004, 4, 437.

[2] K. A. Krohn, J. M. Link,R. P. Mason, The Journal of Nuclear Medicine 2008, 49 Suppl 2, 129s.

[3] R. C. Vannucci, Pediatric Research 1990, 27, 317.

[4] M. Ho¨ckel,P. Vaupel, JNCI: Journal of the National Cancer Institute 2001, 93, 266.

[5] D. J. Yang, S. Wallace, A. Cherif, C. Li, M. B. Gretzer, E. E. Kim,D. A. Podoloff, Radiology 1995, 194, 795.

[6] C. P. Guise, A. T. Wang, A. Theil, D. J. Bridewell, W. R. Wilson,A. V. Patterson, Biochemical Pharmacology 2007, 74, 810.

[7] A. Sahu, W. I. Choi,G. Tae, Advanced Therapeutics 2018, 1, 1800026.

[8] M. Piert, H.-J. Machulla, M. Picchio, G. Reischl, S. Ziegler, P. Kumar, H.-J. Wester, R. Beck, A. J. B. McEwan, L. I. Wiebe,M. Schwaiger, Journal of Nuclear Medicine 2005, 46, 106.

[9] M. Rooseboom, J. N. M. Commandeur,N. P. E. Vermeulen, Pharmacological Reviews 2004, 56, 53.

[10] A. K. Sinhababu,D. R. Thakker, Advanced Drug Delivery Reviews 1996, 19, 241.

[11] R. Zhu, R. P. Baumann, P. G. Penketh, K. Shyam,A. C. Sartorelli, Journal of Medicinal Chemistry 2013, 56, 1355.

[12] R. K. Jain, Scientific American 1994, 271, 58.

[13] C. C. Lee, J. A. MacKay, J. M. J. Fréchet,F. C. Szoka, Nature Biotechnology 2005, 23, 1517.

[14] E. Abbasi, S. F. Aval, A. Akbarzadeh, M. Milani, H. T. Nasrabadi, S. W. Joo, Y. Hanifehpour, K. Nejati-Koshki,R. Pashaei-Asl, Nanoscale Research Letters 2014, 9, 247.

[15] H. Yang,W. J. Kao, Journal of Biomaterials Science, Polymer Edition 2006, 17, 3.

[16] S. Li, M. L. Szalai, R. M. Kevwitch,D. V. McGrath, Journal of the American Chemical Society 2003, 125, 10516.

[17] R. J. Amir, N. Pessah, M. Shamis,D. Shabat, Angewandte Chemie International Edition 2003, 42, 4494.

[18] F. M. H. de Groot, C. Albrecht, R. Koekkoek, P. H. Beusker,H. W. Scheeren, Angewandte Chemie International Edition 2003, 42, 4490.

[19] C. A. Blencowe, A. T. Russell, F. Greco, W. Hayes,D. W. Thornthwaite, Polymer Chemistry 2011, 2, 773.

[20] G. Liu, X. Wang, J. Hu, G. Zhang,S. Liu, Journal of the American Chemical Society 2014, 136, 7492.

[21] A. Warnecke,F. Kratz, The Journal of Organic Chemistry 2008, 73, 1546.

[22] J. S. Robbins, K. M. Schmid,S. T. Phillips, The Journal of Organic Chemistry 2013, 78, 3159.

[23] A. P. Esser-Kahn, N. R. Sottos, S. R. White,J. S. Moore, Journal of the American Chemical Society 2010, 132, 10266.

[24] N. El-Najjar, H. Gali-Muhtasib, R. A. Ketola, P. Vuorela, A. Urtti,H. Vuorela, Phytochemistry Reviews 2011, 10, 353.

[25] L. Cui, Y. Zhong, W. Zhu, Y. Xu, Q. Du, X. Wang, X. Qian,Y. Xiao, Organic Letters 2011, 13, 928.

[26] R. B. Greenwald, A. Pendri, C. D. Conover, H. Zhao, Y. H. Choe, A. Martinez, K. Shum,S. Guan, Journal of Medicinal Chemistry 1999, 42, 3657.

[27] A. Alouane, R. Labruère, T. Le Saux, F. Schmidt,L. Jullien, Angewandte Chemie International Edition 2015, 54, 7492.

[28] V. V. Didenko, BioTechniques 2001, 31, 1106.

[29] M. K. Johansson,R. M. Cook, Chemistry − A European Journal 2003, 9, 3466.

[30] Y. Urano, D. Asanuma, Y. Hama, Y. Koyama, T. Barrett, M. Kamiya, T. Nagano, T. Watanabe, A. Hasegawa, P. L. Choyke,H. Kobayashi, Nature Medicine 2008, 15, 104.

[31] N. G. Zhegalova, S. He, H. Zhou, D. M. Kim,M. Y. Berezin, Contrast Media & Molecular Imaging 2014, 9, 355.

[32] H. v. Berlepsch,C. Böttcher, Physical Chemistry Chemical Physics 2018, 20, 18969.

[33] M. Wang, G. L. Silva,B. A. Armitage, Journal of the American Chemical Society 2000, 122, 9977.

[34] D. Zhu, L. Xue, G. Li,H. Jiang, Sensors and Actuators B: Chemical 2016, 222, 419.

[35] B. A. Teicher,A. C. Sartorelli, Journal of Medicinal Chemistry 1980, 23, 955.

[36] P. L. Carl, P. K. Chakravarty,J. A. Katzenellenbogen, Journal of Medicinal Chemistry 1981, 24, 479.

[37] F. M. H. de Groot, W. J. Loos, R. Koekkoek, L. W. A. van

Berkom, G. F. Busscher, A. E. Seelen, C. Albrecht, P. de Bruijn,H. W. Scheeren, The Journal of Organic Chemistry 2001, 66, 8815.

Chapter 3.

Ultrasound-Mediated Enhanced Drug Delivery by Using Microbubble-Self-Aggregate Complex

3.1. Introduction

Microbubble acts as an ultrasound contrast agent by increasing the contrast of the ultrasound image by causing the scattering of ultrasonic waves.[1], [2], [3], [4], [5] Microbubbles are also contracted and expanded by acoustic pulses, causing flow to the surrounding liquid. When the ultrasonic waves are strong enough, the microbubble collapses and forms strong mechanical stress flow (shockwave) or microjet and call this phenomenon inertial cavitation.[5], [6], [7], [8], [9] Shock waves and microjets can disturb cell membranes or junction of vascular endothelial cell, which can selectively cause increased permeability to local sites by microbubbles and ultrasound.[10], [11], [12] Based on this phenomenon, research is being conducted to selectively deliver drugs to target sites using microbubbles.

In this study, we investigated the possibility of treating prostate cancer by loading hydrophobic drug paclitaxel into microbubbles. Hydrophobic drugs such as docetaxel are restricted to intravenous injection due to low solubility in aqueous solution and many studies are being conducted to improve water solubility.[13], [14] To deliver the hydrophobic drug, hydrophobic drug carriers is required. When loading the hydrophobic drug into the microbubble, the drug loading capacity is low because drugs have to

be loaded into the gas core or microbubble shell. In addition, if the drug was loaded into the microbubble shell, the shell is stabilized, making it difficult to collapse by ultrasonic waves, which requires strong ultrasonic waves to increase the permeability. [15], [16], [17] For effective ultrasound-mediated drug delivery, inertial cavitation of the microbubble should not occur in overly high ultrasound intensity because high ultrasound intensity can cause cell death. It is necessary to conjugate hydrophobic drug carrier with microbubble to form complex to minimize physical property change of microbubble. In this study, self-aggregate was conjugated to microbubble to act as a hydrophobic drug carrier.

When an amphiphilic polymer is present in an aqueous environment, it spontaneously self-assembles a nano-sized structure, at the concentration above a critical point, with a hydrophilic shell surrounding a hydrophobic core to minimize interfacial energy. Glycol chitosan is one of the chitosan derivatives that is completely soluble at neutral pH and contains amino side groups, available for further modification, in each repeating carbohydrate. Glycol chitosan is widely used in pharmaceutical and biomedical applications because of its easy chemical modification, biocompatibility, biodegradability, and low immunogenicity.[18] Glycol chitosan forms self-aggregates in the water when a predetermined percentage of amino groups are modified by a

hydrophobic moiety and the concentration is above a critical point. The hydrophobic drug can be introduced into the hydrophobic core of the self-aggregates via hydrophobic interaction[19], [20] in the process of forming a self-assembled nanostructure. Glycol chitosan self-aggregates could be conjugated with microbubble via the formation of covalent bonds. Glycol chitosan self-aggregates play roles in providing microbubbles with the capacity of hydrophobic drug delivery and in increasing the targeting efficiency into the tumor sites. In case of lipid and albumin based microbubble delivery,[21], [22] most of the microbubbles became accumulated in the liver and lung even in the presence of tumor targeting moiety. When the surface of the microbubbles was modified with glycol chitosan, expected are the decrease in liver and lung accumulation and the increase in tumor targeting of the microbubbles, probably because pKa value of amino groups in glycol chitosan is around 6.8. Glycol chitosan self-aggregates become non-charged in the blood stream, while the aggregates induce positive charges in the acidic microenvironment of tumor tissues.[18], [23], [24], [25] The changes of the charges depending on the pH are expected to endow the glycol chitosan self-aggregates separated from microbubble after ultrasound signal with the better access to the internalization into the tumor cells.[25], [26]

3.2. Experimental

Materials. Glycol chitosan (M_w=350 kDa), N-(3-dimethylaminopropyl)-N′-ethylcarbodiimide (EDC, 97 %), N-hydroxysuccinimide (NHS, 98 %), Sudan III, deoxycholic acid (98 %), anhydrous dimethyl sulfoxide (DMSO), Tween 80, Rhodamine (95 %), dialysis tubing cellulose membrane (Molecular weight cut off: 14 kDa), and . 3-(4,5-dimethylthiazol-2-yl)-2,5-diphenyltetrazolium for MTT assay were purchased from Sigma-Aldrich (St. Louis, MO). Cyanine5.5 NHS ester (Cy5.5-NHS) was commercially available from Lumiprobe (Hunt Valley, Maryland). Methanol (99.5 %) and tetrahydrofuran (99 %) were obtained from Daejung (Korea). 1,2-distearoyl-sn-glycero-3-phosphocholine (DSPC) and 1,2-distearoyl-sn-glycero-3-phosphoethanolamine-N-[succinyl (polyethylene glycol)-2000] (DSPE-PEG2k-NHS) were purchased from NOF Corporation (Tokyo, Japan). All other chemicals were commercially available and used as received.

Instruments. ^{1}H-NMR analysis was performed by Bruker Avance 300 MHz spectrometer in D_2O/CD_3OD at room temperature. Microbubbles (MB) were prepared via a mechanical mixing with a high-speed shaking-

device (KIMS, South Korea). Measurement of particle size and zeta potential were carried out using Otsuka ELS-Z (Otsuka, Japan) instrument equipped with He-Ne laser at a wavelength of 630 nm. UV-visible spectra were obtained by Shimadzu UV-2450 (Shimadzu, Japan). Docetaxel concentration was measured by high performance liquid chromatography (HPLC, Shimadzu) at 25 °C with a reverse-phase C_{18} column (250 X 4.6 mm, 5 μm, C_{18}, TOSOH, Kyoto), with acetonitrile/water (60/40, v/v). The flow rate of mobile phase was 1 mL/min and detected at 220 nm. US imaging was performed with a 5-12 MHz broadband linear transducer (Philips, Bothell, WA, USA), and iU22 US scanner (Philips, Bothell, WA, USA).

Synthesis of deoxycholic acid modified glycol chitosan (DOCA-GC). Glycol chitosan (0.50 g) was dissolved in 50 ml double distilled water for 24 h and diluted with 50 ml methanol in 250 mL round bottom flask. Deoxycholic acid (0.56 g 1.43 mmol), EDC (0.41 g, 2.15 mmol) and NHS (0.25 g, 2.15 mmol) were dissolved in 100 mL methanol and transferred to the glycol chitosan solution. After the reaction mixture was stirred for 24 h at room temperature, the solution was dialyzed for 3 d against the excess amount of water/methanol (1:3 v/v) using a dialysis membrane (MWCO: 14 kDa).[19] The final solution was lyophilized to obtain DOCA-GC powder.

Synthesis of fluorescence dye labeled DOCA-GC. DOCA-GC (50 mg) was dissolved in 20 ml DMSO for 12 h, followed by the addition of Rhodamine (5 mg, 10 μmol), EDC (3.8 mg, 19.9 μmol) and NHS (2.3 mg, 19.9 μmol). The mixture was stirred in the dark atmosphere at room temperature for 24 h. The reaction medium was dialyzed against the excess amount of double distilled water for 1 d using a dialysis membrane (MWCO: 14 kDa) and freeze-dried to obtain Rhodamine labeled DOCA-GC. The UV absorbance of Rhodamine labeled DOCA-GC solutions was measured at the wavelength of 565 nm for determining the amount of conjugated Rhodamine. The conjugation ratio of Rhodamine labeled DOCA-GC was calculated from the absorption with reference to a standard curve constructed with freshly prepared Rhodamine solution.

DOCA-GC (10 mg) was dissolved in 1 ml DMSO for 12 h, followed by the addition of Cy5.5-NHS (0.1 mg, 0.13 μmol) in 10 mL schlenk tube. The mixture was stirred in the dark atmosphere at room temperature for 24 h. The reaction medium was dialyzed against the excess amount of water/methanol (1:3 v/v) for 1 d using a dialysis membrane (MWCO: 14 kDa) to remove unreacted Cy5.5. The resulting product was freeze-dried to obtain Cy5.5 labeled DOCA-GC. The UV absorbance of Cy5.5 labeled DOCA-GC

solutions was measured at the wavelength of 675 nm for determining the amount of conjugated Cy5.5. The conjugation ratio of Cy5.5 labeled DOCA-GC was calculated from the absorption with reference to a standard curve constructed with freshly prepared Cy5.5 solution.

Preparation of deoxycholic acid modified glycol chitosan self-aggregates (DOCA-GC SA). DOCA-GC SA was produced by simple sonication method. DOCA-GC (20 mg) was dispersed in 10 ml PBS buffer (pH 7.4) at 37 °C during 12 h. The mixture was sonicated using a probe-type sonicator (Cole parmer ultrasonic processor) for 20 min under an ice bath to minimize the increase of temperature. The resulting mixture was filtered through a 0.8 μm PTFE syringe filter to obtain DOCA-GC SA. Cy5.5 and Rhodamine labeled DOCA-GC SA also prepared in the same process as described above.

Preparation of docetaxel and Sudan III loaded DOCA-GC. Docetaxel was dissolved in ethanol (40 mg / mL). Docetaxel solution (100 μL) was added dropwise into DOCA-GC SA aqueous solution (10 mL, 2 mg / mL) under sonication by using probe-type sonicator for 15 min under an ice bath. The solution was filtered through a 0.8 μm PTFE syringe filter to

remove unloaded drugs. Drug loading amount and efficiency were measured by high performance liquid chromatography (HPLC).

Sudan III solution in THF (100 μL, 1 mg / mL) was added dropwise into DOCA-GC SA aqueous solution (10 mL, 2 mg / mL) under sonication by using probe-type sonicator for 15 min under an ice bath. The solution was filtered through a 0.8 μm PTFE syringe filter to remove unloaded Sudan III. The UV absorbance of the resulting aqueous solution was measured at the wavelength of 500 nm for determining the amount of loaded Sudan III.

$$\text{Loading efficiency (\%)} = \frac{\text{Amount of loaded in self-aggregates}}{\text{Amount of the feeding}} \times 100\ (\%) \quad (1)$$

$$\text{Loading amount (\%)} = \frac{\text{Weight of loaded drugs}}{\text{Weight of self-aggergates+loaded drugs}} \times 100\ (\%) \quad (2)$$

In vitro drug release profile of docetaxel loaded DOCA-GC. Freshly prepared docetaxel loaded DOCA-GC SA aqueous solution (2 mL, 2 mg / mL) in a dialysis bag (MWCO: 14 kDa) was placed in a conical tube containing 20 mL phosphate buffer saline (PBS, pH 7.4) with 0.1 wt % tween80 as a release media. The system was maintained at 37 °C with shaking (80 rpm), the release media was replaced by fresh incubation medium at predetermined time points. The drug in the incubation medium was measured

by HPLC.

Preparation of NHS-functionalized MB. NHS-functionalized MBs were developed by sulfur hexafluoride (SF_6) gas and stabilized with 2 kinds of phospholipids, DSPC for main structure and DSPE-PEG2k-NHS for binding group to DOCA-GC SA. Synthesis of MBs were basically followed to reverse phase transition method. DSPC and DSPE-PEG2k-NHS with the molar ratio of 9:1 were dissolved to chloroform and fully evaporated by rotary evaporation for 30 min. And this phospholipid thin film was hydrated by phosphate buffered saline (0.01 M, pH 7.4) under the phase transition temperature of DSPC (55-60 °C). The phospholipid hydrates were dissolved at the concentration of 1 mg/mL. To be prepared to uni-lamellar structure, the phospholipid hydrates were immediately bath-sonicated for 1 min. After sonication, head space of vial was filled with the SF_6 gas. Sequentially, this phospholipid hydrates were strongly agitated for transformation to MB by VialMIX for 45 seconds. Size of MB were measured by Dynamic light scattering method. Optical and fluorescence images of MBs were obtained under a phase-contrast microscope with a 40× objective (CKX41, Olympus Co. Ltd., Tokyo, Japan).

Preparation of MB-DOCA-GC SA. 1 mL DOCA-GC SA in PBS buffer (2.0 mg / mL) were injected into a 2.5 mL vial containing 1 mL NHS-modified MB in PBS buffer (1.0 mg/mL, 5 x 10^9 MB / mL). The reaction mixture underwent gentle shaking for 1 h at room temperature. After the reaction completed, unreacted DOCA-GC SA was removed by centrifugation (3,000 rpm, 15 min).

Identify self-aggregate conjugation ratio of MB. Sudan III loaded MB-DOCA-GC SA complex was prepared in the same process as described above. The concentration of unreacted Sudan III loaded SA in the supernatant was calculated from the absorption with reference to a standard curve constructed with freshly prepared Sudan III solution. Sudan III loaded SA conjugation ratio (%) was calculated from the following equation.

$$\text{Conjugation ratio (\%)} = \left(1 - \frac{\text{Sudan III load SA in supernatant}}{\text{Total Sudan III loaded SA}}\right) \times 100\ (\%)$$

In vitro ultrasound image of MB-DOCA-GC SA. MB-DOCA-GC SA or free MB were transferred to an Eppendorf tube. MB-DOCA-GC SA filled Eppendorf tube was positioned in the chamber filled with water (200 mL) to evaluate echogenicity. US imaging was performed with a 5-12 MHz

broadband linear transducer and iU22 US scanner. Acoustic pressure was measured based on the mechanical index (MI) and MI for measuring echogenicity was 0.08. The ultrasonic image signal attenuation behavior was verified by evaluating echogenicity after performing several flash condition (MI = 0.61, 0.5 s).

Ultrasound triggered intracellular delivery of MB-DOCA-GC SA complex. 3×10^4 cells (LNCap or PC3) were seeded in the wells of a 48-well plate (BD Falcon) or confocal 4-well plate (Lab-tex, NY, USA) before 24 h. Rhodamine labeled MB-DOCA-GC SA was added to cells in culture media containing 10 % fetal bovine serum (FBS). Following ultrasound irradiation, the cell was incubated with MB-DOCA-GC SA for 3 h or 6 h. The probe was placed in backside of the well plate and ultrasound were performed for 10 minutes (1 MHz, 1 W/cm^2). After incubation, MB-DOCA-GC SA complex was washed out with PBS solution and cell line was visualized by confocal microscopy.

In vitro cell viability test. MTT assay was used to evaluate cell viability in the presence of MB, free docetaxel and docetaxel loaded MB-DOCA-GC SA complex. PC3 cells (KCLB, Seoul, Korea) were cultured in

RPMI supplemented with FBS (10 %) and penicillin and streptomycin (1 %). Cells were maintained at 37 °C in a humidified atmosphere containing 5 % CO_2. At confluence, the cells were washed, trypsinized, and re-suspended in culture media. Cells were then seeded at a concentration of 5,000 cells/well in a 96-well tissue culture plate and allowed to grow overnight at 37 °C under 5 % CO_2. MB, free docetaxel and MB-DOCA-GC SA were transferred to cells in culture media, and irradiate ultrasound for 10 minutes (1 MHz, 1 W/cm^2). The cells were incubated another 72 h. After incubation, the medium was substituted with MTT solution and incubation for another 3 h at 37 °C under 5 % CO_2. The media were removed and resulting formazan crystal was dissolved in DMSO. UV absorbance at 570 nm was measured with a microplate reader.

Ultrasound imaging and ex vivo biodistribution. PC3 cells (1.5×10^6) cultured in RPMI containing 10 % FBS, penicillin and streptomycin were injected subcutaneously into the hind leg muscle of mice (BALB/C, 6-7 week old, male). When the tumor had grown to 10-15 mm in size, 300 μL Cy5.5 labeled MB-DOCA-GC SA (3 mg / mL) was intravenously injected through a tail vein. Ultrasound imaging was obtained with an iU22 ultrasound scanner equipped with a 5- to 12-MHz broadband

linear transducer. Two minutes after injection of Cy5.5 labeled MB-DOCA-GC SA, flashes with a mechanical index of 0.61 were performed during 10 minutes. After 24 h later, the following were collected in all animals: liver, lung, spleen, kidney, heart, tumor. Tissues were evaluated by NIRF tomographic images with Kodak imaging station with Cy5.5 excitation filter.

3.3. Results and discussion

Glycol chitosan and deoxycholic acid were successfully conjugated by EDC-NHS reaction and characterized by ^{1}H-NMR. EDC and NHS catalyze the formation of the amide linkage between the carboxylic group of deoxycholic acid and primary amine groups in glycol chitosan. Conjugation ratio of glycol chitosan and deoxycholic acid were determined by ^{1}H NMR analysis.[19], [27] 19.3 ± 1.24 % of amine group was substituted to deoxycholic acid by comparing of ^{1}H NMR Intensity of glycol chitosan region (3.9-3.3 ppm) and deoxycholic acid region (0.9-0.5 ppm). ^{1}H NMR results were reproducible over 3 separate experiments (Figure 3-1).

Rhodamine was successfully conjugated onto the DOCA-GC in the presence of EDC and NHS as catalysts. Cy5.5-NHS was successfully introduced into the DOCA-GC. After dissolving of Rhodamine or Cy5.5 labeled DOCA-GC in aqueous solution, we estimated that 8.4 molecules of Rhodamine or 4.5 molecules of Cy5.5 were chemically conjugated, confirmed by the absorption curve of Rhodamine at 565 nm or Cy5.5 at 675 nm.

DOCA-GC has a hydrophilic main chain and a hydrophobic deoxycholic side group to form a self-aggregate structure in which

hydrophobic deoxycholic acid is aggregated to minimize exposure to the aqueous solution. The size of DOCA-GC SA measured by DLS was 310.7 ± 53.8 nm and the zeta potential of 10.8 mV. (Figure 3-2A) Rhodamine and Cy5.5 labeled DOCA-GC SA show 310.0 ± 81.8 nm and 329.1 ± 97.4 nm. (Figure 3-2D, 3-2E)

Docetaxel and Sudan III could be successfully incorporated into DOCA-GC SA by sonication method.[28] DOCA-GC has hydrophobic inner cores consist of hydrophobic deoxycholic acid. Hydrophobic compound could be loaded into the self-aggregates hydrophobic core by hydrophobic interaction. Both Docetaxel and Sudan III were successfully loaded into glycol chitosan self-aggregates by sonication method. Generally, it was reported that the drug loading amount of docetaxel and Sudan III was about 10 to 20 %[29], [30] and 0.9 %[31], [32] in the nanoparticles, respectively. As shown in Figure 3-2 and Table 3-1, Sudan III loaded DOCA-GC SA show 337.0 ± 45.3 nm, 17 % of loading efficiency and 0.76 % of loading amount and Docetaxel loaded DOCA-GC SA show 323.0 ± 26.5 nm, 83.2 % of loading efficiency and 26.0 % of loading amount.

Figure 3-3 showed the in vitro release profile of docetaxel loaded DOCA-GC SA. The time dependent release of docetaxel form docetaxel loaded DOCA-GC SA was determined in the sink condition with 0.1 % tween

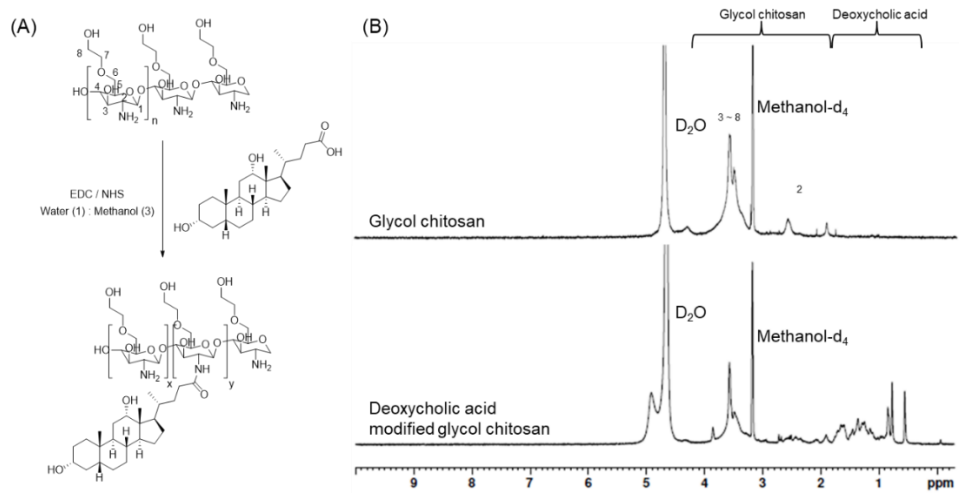

Figure 3-1. (A) Scheme for the synthesis of DOCA-GC, (B) corresponding ^{1}H NMR spectra in D_2O/CD_3OD (1:1 v/v)

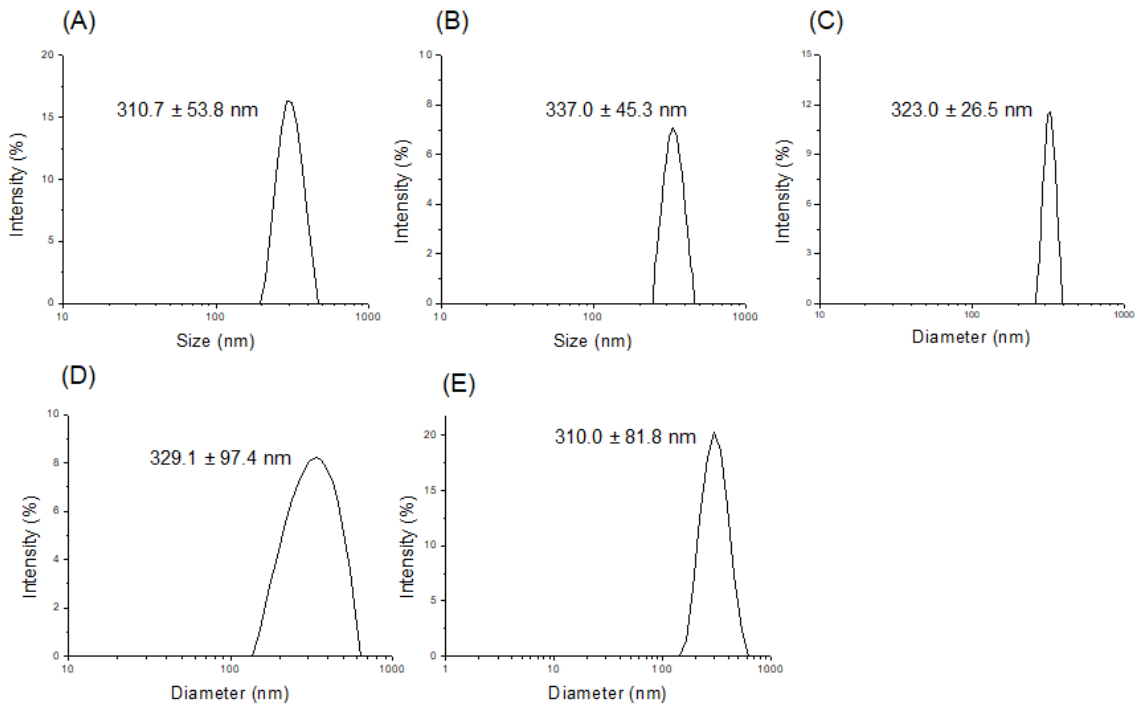

Figure 3-2. Size distribution of SAs. (A) DOCA-GC SA, (B) Sudan III loaded DOCA-GC SA, (C), docetaxel loaded DOCA-GC SA, (D) Cy5.5 labeled DOCA-GC SA, (E) Rhodamine labeled DOCA-GC SA.

Table 3-1. Physical characteristics of docetaxel and Sudan III loaded DOCA-GC SA.

	Size (nm)	Efficiency (%)	Amount (%)
Glycol chitosan SA	310.7 ± 53.8 nm	-	-
Docetaxel loaded DOCA-GC SA	323.0 ± 26.5 nm	83.2 ± 0.8	26.0 ± 0.7
Sudan III loaded DOCA-GC SA	337.0 ± 45.3 nm	17.0 ± 0.6	0.76 ± 0.1

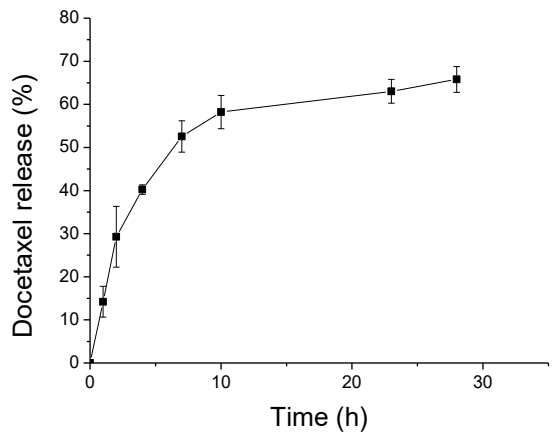

Figure 3-3. In vitro docetaxel release profile from DOCA-GC SA at 37 °C.

80 in PBS buffer. The release profile shows typical two-phase release patterns. 60 % of docetaxel was rapidly released first 10 hours, followed by a slower and continuous release.

MB was prepared by redissolving lyophilized phospholipid film in an aqueous buffer in the presence of SF_6 gas under intense shaking. Prepared MB has 1 ~ 2 μm size which was modified with NHS groups for conjugation with DOCA-GC SA. DOCA-GC SA and MBs were chemically conjugated by reaction with the amine group of glycol chitosan self-aggregates and NHS ester functionalized at the surface of the MB. As mentioned above experiment procedure, conjugation ratio of DOCA-GC SA was measured by Sudan III loaded DOCA-GC SA. Concentration of Sudan III in the supernatant indicate that the conjugation ratio of DOCA-GC SA with MBs which was 73.9 % (Figure 3-4). In addition, after conjugation of Rhodamine labeled DOCA-GC SA with MBs and confirming them with confocal microscopy, it can be directly confirmed that SA was conjugated to MB surface (Figure 3-5A).

The ultrasound imaging ability of MB-DOCA-GC SA was compared with MB under the same conditions. As shown in Figure 3-6, MB-DOCA-GC SA shows similar ultrasound echogenicity with MBs and signal reduction behavior under the flash pulses. These results show that the self-aggregate introduced on the MB surface does not affect the ultrasonic behavior of the

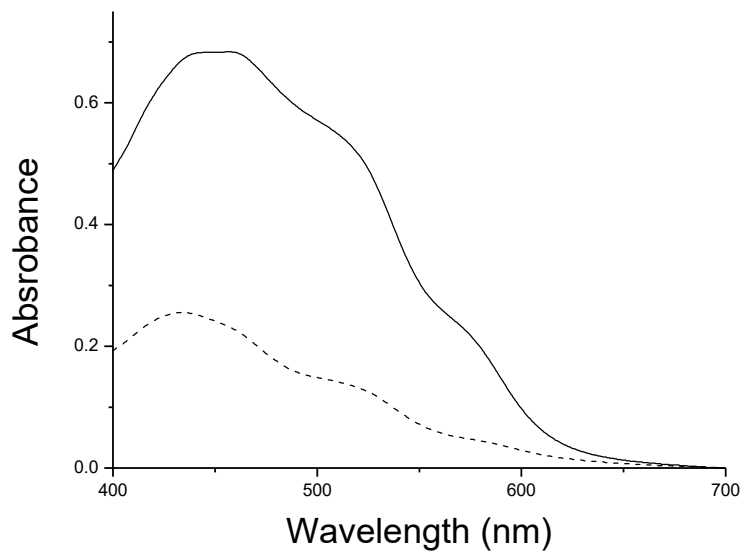

Figure 3-4. UV-vis spectroscopy data of Sudan III loaded DOCA-GC SA. The control group (solid line), remaining Sudan III loaded DOCA-GC SA in the supernatant after conjugation (dash).

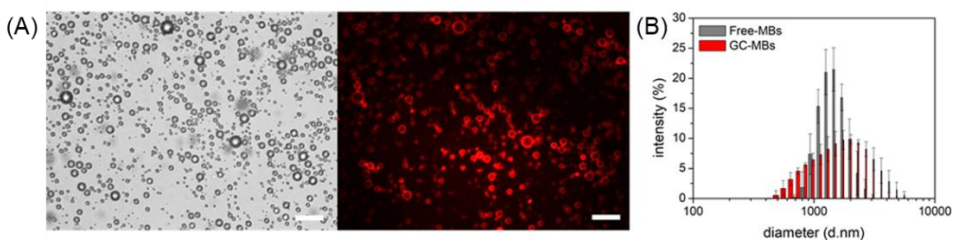

Figure 3-5. A) Confocal microscopy Image of Rhodamine labeled DOCA-GC SA, B) Size distribution of Rhodamine labeled DOCA-GC SA

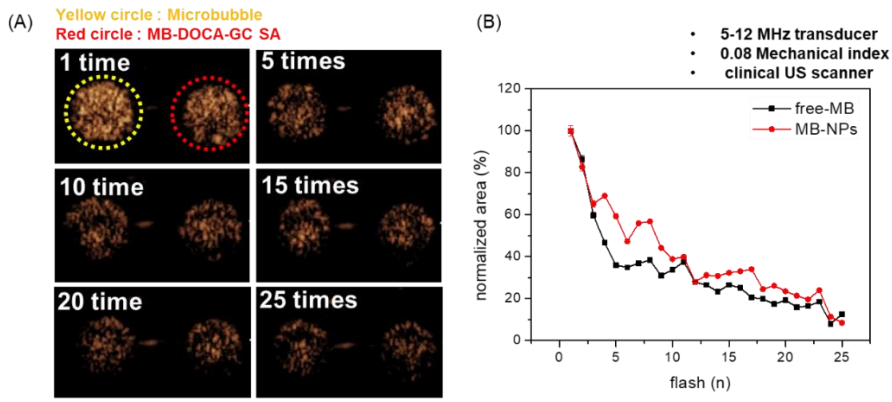

Figure 3-6. (A) Ultrasound image of MB-DOCA-GC SA by frequency of ultrasound flash, (B) normalized area of ultrasound signal

MB. Previous studies have confirmed that the lipid-based MB encapsulated with SF_6 gas has an ultrasound imaging capability similar to that of the SonoVue®,[12] a commercialized ultrasound contrast agent, so that ultrasound imaging effects can be obtained effectively even in vivo conditions.

MB could improve the permeability of the cell membrane under the ultrasound irradiation. Rhodamine labeled MB-DOCA-GC SA was used for monitoring cellular uptake enhancement in the presence or absence of ultrasound activation. Confocal microscopy showed cellular uptake behavior of Rhodamine labeled MB-DOCA-GC SA. Both LNcap and PC3 cell line confirmed that the Rhodamine-labeled MB-DOCA-GC SA penetrated into the cells effectively within a short period of time and confirmed the enhancement of permeability by ultrasound irradiation (Figure 3-7A).

The cell viability of the PC3 cell line was confirmed by MTT assay by treating MB, free docetaxel and MB-DOCA-GC SA. Blank PC3 cell line and MB treated PC3 cell line showed no significant change in cell viability, regardless of whether they were irradiated with ultrasound flash. This indicates that the ultrasound used in the experiment and that transient cell membrane collapse caused by inertial cavitation does not affect cell viability. In the case of Docetaxel treated PC3 cell line, the same cell viability was indicated regardless of ultrasound flash. Docetaxel loaded MB-DOCA-GC

SA shows a significant increase in anti-cancer effect when irradiated with ultrasound. (Figure 3-7B) This shows that there was no cell toxicity due to ultrasound, and the anticancer effect was increased due to improved drug delivery by enhanced cell permeability.

In vivo ultrasound image of PC3 tumor bearing mice were performed at 10 s, 30 s, 60 s and 90 s after the injection of MB-DOCA-GC SA using the clinical ultrasound imaging system iU22 Ultrasound scanner. The acoustic pressure (MI) was 0.07, and frequency of 7 MHz was used for visualizing tumor region. After 10 seconds, the MB induced increase in the ultrasonic signal was observed in the tumor vessels. After 30 seconds, the entire tumor was visualized. MB-DOCA-GC SA reaches the tumor site within a short period of time (Figure 3-8A). When the ultrasound flash was applied to the target site 60 seconds after the injection, ultrasound mediated drug delivery can be effectively performed.

Based on the confirmed ultrasound mediated enhanced permeability in vitro, we conducted an experiment to confirm the increase of tumor delivery efficiency by ultrasound flash using PC3 tumor-bearing mouse model. Mice model were sacrificed 24 hours after intravenous injection of Cy5.5 labeled MB-DOCA-GC SA. Excised organs from MB-DOCA-GC SA administered mice were evaluated by Kodak imaging station. Among the

excised organs, the fluorescence signal of the liver is the highest, and in the organs except the tumor, there is no significant difference according to the before and after the ultrasonic flash. When ultrasound flash was applied to the tumor site, the fluorescence signal increased twice as compared to non-flash (Figure 3-8B). The shockwave by inertial cavitation not only temporarily disrupts the cell membrane but also loosens junction of the vascular endothelial cell, allowing MB-DOCA-GC SA to reach the tumor region and inside of the tumor cell. It seems that the amount transferred to the tumor increased due to local permeability around the tumor by ultrasonic flash. In our previous research,[12] Liposome MBs tend to be transmitted in high proportions to liver and lung. In this experiment, the rate of uptake in the liver is still high, but the rate of uptake in the lung is low. Lipid or albumin based MBs are known to cause phagocytosis by macrophages.[33], [34], [35] MB-DOCA-GC SA has been modified with glycol chitosan to inhibit phagocytosis caused by alveolar macrophages, which are present in a fixed form in the lungs, suggesting that lung uptake is reduced.

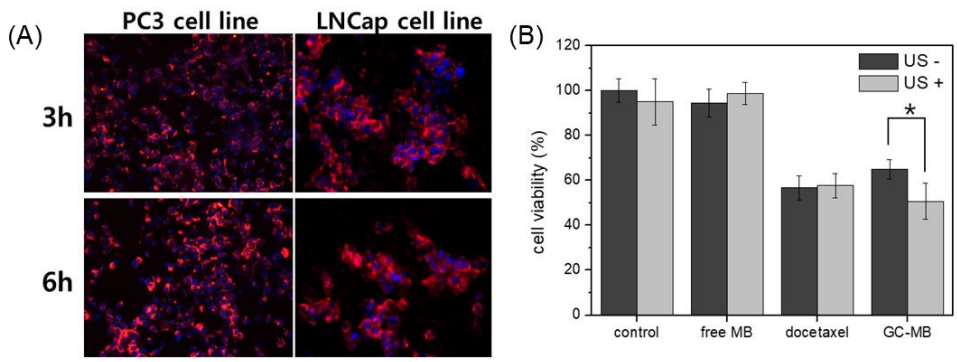

Figure 3-7. (A) Optical image after ultrasound flash in the presence of MB-DOCA-GC SA , (B) cell viability of PC3 cell line treated with blank, free MB, free docetaxel and MB-DOCA-GC SA with or without ultrasound flash.

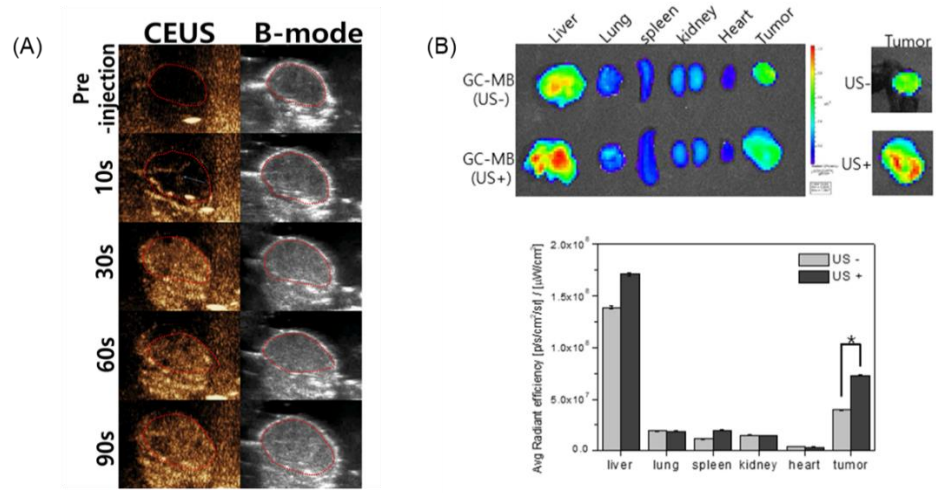

Figure 3-8. (A) In vivo ultrasound image of tumor after intravenous injection of MB-DOCA-GC SA, (B) ex vivo fluorescence image after intravenously injection of MB-DOCA-GC SA with or without ultrasound flash.

3.4. Conclusion

Hydrophobic drug loaded MB-SA complex was synthesized while maintaining the echogenicity and inertial cavitation condition of MB. MB-DOCA-GC SA exhibits selective cell permeability enhancement at the target site by ultrasound flash and showed an increase in anti-cancer effect in ultrasound flash condition at in vitro condition. We also observed the enhancement of MB-DOCA-GC SA transfer ratio by ultrasonic flash at ex vivo condition. In future studies, targeting moiety will be introduced to increase selectivity for tumor and visualize tumor grow inhibition at in vivo condition.

3.5. Reference

[1] J. G. Riess, Current Opinion in Colloid & Interface Science 2003, 8, 259.

[2] J. R. Lindner, Nature Reviews Drug Discovery 2004, 3, 527.

[3] R. S. Meltzer, E. G. Tickner, T. P. Sahines,R. L. Popp, J. Clin. Ultrasound 1980, 8, 121.

[4] I. Lentacker, S. C. De Smedt,N. N. Sanders, Soft Matter 2009, 5, 2161.

[5] K. Ferrara, R. Pollard,M. Borden, Annu. Rev. Biomed. Eng. 2007, 9, 415.

[6] H. L. Liu, C. H. Fan, C. Y. Ting,C. K. Yeh, Theranostics 2014, 4, 432.

[7] L. M. Tay,C. Xu, Nanomedicine 2017, 12, 91.

[8] S. Hernot,A. L. Klibanov, Adv. Drug Del. Rev. 2008, 60, 1153.

[9] E. Unger, T. Porter, J. Lindner,P. Grayburn, Adv. Drug Del. Rev. 2014, 72, 110.

[10] J. J. Choi, J. A. Feshitan, B. Baseri, S. Wang, Y. S. Tung, M. A. Borden,E. E. Konofagou, IEEE Trans. Biomed. Eng. 2010, 57, 145.

[11] J. Song, P. S. Cottler, A. L. Klibanov, S. Kaul,R. J. Price, Am. J. Physiol. Heart Circ. Physiol. 2004, 287, H2754.

[12] Y. I. Yoon, Y. S. Kwon, H. S. Cho, S. H. Heo, K. S. Park, S. G. Park, S. H. Lee, S. I. Hwang, Y. I. Kim, H. J. Jae, G. J. Ahn, Y. S. Cho, H. Lee, H. J. Lee,T. J. Yoon, Theranostics 2014, 4, 1133.

[13] K. Fuhrmann, J. D. Schulz, M. A. Gauthier,J.-C. Leroux, ACS Nano 2012, 6, 1667.

[14] P.-F. Cui, W.-R. Zhuang, X. Hu, L. Xing, R.-Y. Yu, J.-B. Qiao, Y.-J. He, F. Li, D. Ling,H.-L. Jiang, Chem. Commun. 2018, 54, 8218.

[15] K. Kooiman, M. R. Böhmer, M. Emmer, H. J. Vos, C. Chlon, W. T. Shi, C. S. Hall, S. H. P. M. de Winter, K. Schroën, M. Versluis, N. de Jong,A. van Wamel, J. Controlled Release 2009, 133, 109.

[16] M. J. Shortencarier, P. A. Dayton, S. H. Bloch, P. A. Schumann, T. O. Matsunaga,K. W. Ferrara, IEEE transactions on ultrasonics, ferroelectrics, and frequency control 2004, 51, 822.

[17] E. C. Unger, T. P. McCreery, R. H. Sweitzer, V. E. Caldwell,Y. Wu, Investigative radiology 1998, 33, 886.

[18] J. Y. Yhee, S. Son, S. H. Kim, K. Park, K. Choi,I. C. Kwon, J. Controlled Release 2014, 193, 202.

[19] S. Kwon, J. H. Park, H. Chung, I. C. Kwon, S. Y. Jeong,I.-S. Kim, Langmuir 2003, 19, 10188.

[20] S. J. Lee, H. S. Min, S. H. Ku, S. Son, I. C. Kwon, S. H. Kim,K. Kim,

Nanomedicine 2014, 9, 1697.

[21] A.-H. Liao, S.-Y. Wu, H.-E. Wang, C.-H. Weng, M.-F. Wu,P.-C. Li, Ultrasonics 2013, 53, 320.

[22] J. K. Willmann, Z. Cheng, C. Davis, A. M. Lutz, M. L. Schipper, C. H. Nielsen,S. S. Gambhir, Radiology 2008, 249, 212.

[23] Y. J. Son, J.-S. Jang, Y. W. Cho, H. Chung, R.-W. Park, I. C. Kwon, I.-S. Kim, J. Y. Park, S. B. Seo, C. R. Park,S. Y. Jeong, J. Controlled Release 2003, 91, 135.

[24] J. H. Na, H. Koo, S. Lee, K. H. Min, K. Park, H. Yoo, S. H. Lee, J. H. Park, I. C. Kwon, S. Y. Jeong,K. Kim, Biomaterials 2011, 32, 5252.

[25] I.-C. Sun, J. H. Na, S. Y. Jeong, D.-E. Kim, I. C. Kwon, K. Choi, C.-H. Ahn,K. Kim, Pharm. Res. 2014, 31, 1418.

[26] S. H. Crayton,A. Tsourkas, ACS Nano 2011, 5, 9592.

[27] Stephen Barnes,D. N. Kirk, The Bile Acids : Chemistry, Physiology, and Metabolism. Plenum Press: New York, 1988; p 68.

[28] H. Kang, J.-D. Kim, S.-H. Han,I.-S. Chang, J. Controlled Release 2002, 81, 135.

[29] Z. Xu, L. Chen, W. Gu, Y. Gao, L. Lin, Z. Zhang, Y. Xi,Y. Li, Biomaterials 2009, 30, 226.

[30] L. Mei, Y. Zhang, Y. Zheng, G. Tian, C. Song, D. Yang, H. Chen, H.

Sun, Y. Tian, K. Liu, Z. Li,L. Huang, Nanoscale Research Letters 2009, 4, 1530.

[31] E. S. Lee, Y. T. Oh, Y. S. Youn, M. Nam, B. Park, J. Yun, J. H. Kim, H.-T. Song,K. T. Oh, Colloids Surf. B. Biointerfaces 2011, 82, 190.

[32] K. T. Oh, T. K. Bronich,A. V. Kabanov, J. Controlled Release 2004, 94, 411.

[33] R. Lindner Jonathan, A. Dayton Paul, P. Coggins Matthew, K. Ley, J. Song, K. Ferrara,S. Kaul, Circulation 2000, 102, 531.

[34] S. Sirsi, J. Feshitan, J. Kwan, S. Homma,M. Borden, Ultrasound Med. Biol. 2010, 36, 935.

[35] R. Lindner Jonathan, J. Song, F. Xu, L. Klibanov Alexander, K. Singbartl, K. Ley,S. Kaul, Circulation 2000, 102, 2745.

국문 요약

질병의 정확한 진단과 조기치료를 위해 효과적인 질병의 영상화 방법의 필요성이 요구되어왔다. 기능적 영상화 방법은 질병에서 발생하는 특이적인 환경을 이용하여 영상화 정보를 얻으므로 질병의 초기단계에서도 효과적인 영상화가 가능하다. 이러한 기능적 영상화를 이용한 분자영상은 암세포를 진단하기 위해 많은 연구가 진행되고 있으며 암세포 주위에서 나타나는 특이적인 환경을 이용하여 선택적인 영상화를 수행할 수 있다. 자극 감응형 물질을 이용하면 암 주위에서 발현되는 환경에 의해 선택적인 질병의 영상화 및 치료물질의 전달이 가능하다. 자극 감응형 물질은 체내 질병에서 발현되는 미세환경에 의해 물리적 성질이 변하거나 화학적으로 변화하는 물질을 말한다.

본 연구에서는 자극 감응형 물질을 이용하여 형광 활성화 프로브를 개발하고자 하였음. 형광물질을 이용한 이미징을 수행하려면 형광 노이즈를 최대한 억제하여야 함. 형광물질을 아무런 조치 없이 사용할 경우 표적 부위의 신호가 배경에 가려

제대로 영상화 되지 않을 가능성이 높으므로 FRET 현상을 이용하여 형광을 소광시킨다. 소광은 형광체와 소광물질이 가까이 접근하는 경우 일어나므로 효소, pH 등과 같은 미세환경에 의해 분해되도록 하여 선택적인 영상화를 수행하는 연구가 진행되고 있음.

자기붕괴구조체는 한 번의 자극으로 연쇄붕괴되어 여러 개의 물질을 방출한다. 두 번째 단원에서는 자기붕괴구조체를 이용하여 저산소 조건에서 선택적으로 형광을 활성화하는 덴드리머 형태의 형광조영물질을 개발하였음. 덴드론 말단에 자기소광이 가능한 형광물질을 결합하여 소광된 상태의 조영제를 합성하였다. 저산소 조건에서 니트로기가 아민기로 환원됨에 따라 연쇄붕괴되어 덴드론 말단의 형광물질을 방출하여 형광 복원 거동을 확인하였다. 형광세기 증가를 통해 저산소 조건의 영상화가 가능하고 일반적인 형광 활성화 프로브와 달리 여러 개의 형광물질을 방출하여 신호를 증폭하는 역할을 기대할 수 있어 저산소 조건을 갖는 암세포의 효과적인 진단 가능성을 나타내었다.

외부에서 자극을 가할 경우 목표 부위에 선택적인 미세환경 변화를 유도할 수 있다. 세 번째 단원에서는 초음파와 마이크로버블에 의해 표적 부위의 세포 투과도를 높여 약물전달 효율을 높이는 것을 확인하였다. 마이크로버블은 초음파 캐비테이션에 의해 마이크로젯으로 명명되는 강한 미세기류를 형성하여 세포막의 일시적인 투과도 증가를 유도할 수 있음. 마이크로버블에 약물전달체를 결합하여 체내에 주사한 후 목표 부위에 초음파를 조사하면 초음파가 조사된 부위에 선택적으로 세포 투과도가 증가하므로 선택적인 약물 전달이 가능하다. 세포 수준에서 마이크로버블 복합체가 초음파에 의해 세포 투과도를 높이는 것을 확인하였으며 동물 실험을 통해 초음파 조사 부위에 약물 전달 효율이 높아지는 것을 형광 영상화를 통해 확인하였다.

주요어 : 자극감응형 재료, 허혈성, 저산소 조건, 자기붕괴구조체, 형광영상화, 마이크로버블, 초음파, 자가 집합체

학 번 : 2011-23323